Scission-point model of nuclear fission based on deformed-shell effects*

B. D. Wilkins, E. P. Steinberg, and R. R. Chasman
Chemistry Division, Argonne National Laboratory, Argonne, Illinois 60439
(Received 1 June 1976)

A static model of nuclear fission is proposed based on the assumption of statistical equilibrium among collective degrees of freedom at the scission point. The relative probabilities of formation of complementary fission fragment pairs are determined from the relative potential energies of a system of two nearly touching, coaxial spheroids with quadrupole deformations. The total potential energy of the system at the scission point is calculated as the sum of liquid-drop and shell- and pairing-correction terms for each spheroid, and Coulomb and nuclear potential terms describing the interaction between them. The fissioning system at the scission point is characterized by three parameters—the distance between the tips of the spheroids (d), the intrinsic excitation energy of the fragments (τ_{int}), and a collective temperature (T_{coll}). No attempt is made to adjust these parameters to give optimum fits to experimental data, but rather, a single choice of values for d, τ_{int}, and T_{coll} is used in the calculations for all fissioning systems. The general trends of the distributions of mass, nuclear charge, and kinetic energy in the fission of a wide range of nuclides from Po to Fm are well reproduced in the calculations. The major influence of the deformed-shell corrections for neutrons is indicated and provides a convenient framework for the interpretation of observed trends in the data and for the prediction of new results. The scission-point configurations derived from the model provide an interpretation of the "saw-tooth" neutron emission curve as well as previously unexplained observations on the variation of $\overline{TKE}$ for isotopes of U, Pu, Cm, and Cf; structure in the width of total kinetic energy release as a function of fragment mass ratio; and a difference in threshold energies for symmetric and asymmetric mass splits in the fission of Ra and Ac isotopes. In spite of a number of recognized simplifications in the model, quantitative fits to the data are generally within expected errors of the shell corrections determined by the Strutinski prescription.

[NUCLEAR REACTIONS, FISSION Po, Ra, U, Cm, Cf, Fm; calculated A, Z, and KE distribution of fragments. Liquid-drop model. Deformed-shell corrections. Strutinski prescription. Asymmetric and symmetric fission.]

I. INTRODUCTION

A satisfactory theoretical interpretation of the asymmetric mass distribution observed in nuclear fission at low excitation energies has been sought since the discovery of this complex nuclear reaction. Although a rough correlation of the most probable mass division with ground-state nuclear closed-shell configurations was recognized, it was not until the development of the shell-correction method of calculating shell effects for the deformed nuclear shapes encountered in the process of fission[1] that a significant breakthrough in understanding began to emerge.

Calculations[2,3] of the potential energy surfaces for fissioning nuclei indicate the importance of the shell correction at deformations corresponding to the second saddle point and qualitatively account for an asymmetric division of mass. On the other hand, calculations employing a two-center model[4-6] indicate that the influence of the nascent fragment shells at deformations near the scission point also favors mass asymmetry in fission. Other scission-point models of fission have been proposed, including statistical calculations,[7] a semiequilibrium approach,[8] and a two-spheroid model.[9] Although all of these treatments give qualitative agreement with some of the observed distributions of fragment mass, kinetic energy, etc., in fission, the fundamental question of when in the process the distributions are determined (i.e., at the second saddle point, at the scission point or somewhere in between) remains unanswered. The treatment of Pashkevich[10] indicates that the mass asymmetry is greatest at the second saddle point and then gradually decreases to the experimentally observed value at the scission point. The importance of the dynamical aspects of fission on these distributions is also unknown and is now receiving more attention[11,12] stimulated by the interest in heavy-ion fusion reactions.

In a previous publication,[13] we presented an interpretation of the mass and charge distributions of fission fragments based on a potential energy calculation for the particular scission-point configuration of two nearly tangent coaxial spheriods. The quadrupole deformations, β_L and β_H, for the light and heavy fragment pair which gave the minimum in the potential energy surface were deter-

mined. The relative potential energies of all other complementary pairs were then calculated at these values of β_L and β_H. The results of that calculation were encouraging and indicated that a surprisingly large number of the observable phenomena of fission, including the mass and charge distributions, could be described by such a static, deformed-shell model of the process.

The present work represents an extension of the previous model to include contributions from all quadrupole deformations of the nascent fragments at the scission point for each mass split. In addition, a nuclear interaction term between the fragments has been added to provide an estimate of the energy associated with the neck region. An improved set of single-particle levels has also been utilized for the calculation of deformed-shell corrections with the Strutinski prescription.

This work should be viewed from the perspective of an evaluation of how successful such a static, scission-point interpretation can be in accounting quantitatively for a wide variety of phenomena observed in nuclear fission and in providing a basis for extrapolations to new fissioning systems and a guide to new experiments.

II. MODEL

The basic assumption of the model used is that the fission fragment distributions can be determined at or near the scission point from the relative potential energies of the complementary nascent fragment pairs. These energies are calculated as functions of their respective neutron and proton numbers (N_1, N_2, Z_1, and Z_2) and deformation parameters (β_1 and β_2). The fragment pairs are treated as nearly touching, coaxial spheroids and an approximation is included for the surface energy associated with the neck connecting them.

The total potential energy of the system at the scission point is treated as a sum of liquid-drop (collective) and shell- and pairing-correction (single-particle) terms for each spheroid with Coulomb and nuclear potential terms describing the interaction between the two coaxial spheroids whose tips are separated by a distance d. The total potential is given by

$$\begin{aligned} V(N_1, Z_1, \beta_1, N_2, Z_2, \beta_2, \tau, d) = {} & V_{\mathrm{LD}_1}(N_1, Z_1, \beta_1) + V_{\mathrm{LD}_2}(N_2, Z_2, \beta_2) \\ & + S_1(N_1, \beta_1, \tau) + S_1(Z_1, \beta_1, \tau) + S_2(N_2, \beta_2, \tau) + S_2(Z_2, \beta_2, \tau) \\ & + P_1(N_1, \beta_1, \tau) + P_1(Z_1, \beta_1, \tau) + P_2(N_2, \beta_2, \tau) + P_2(Z_2, \beta_2, \tau) \\ & + V_C(N_1, Z_1, \beta_1, N_2, Z_2, \beta_2, d) + V_n(N_1, Z_1, \beta_1, N_2, Z_2, \beta_2, d), \end{aligned} \tag{1}$$

where N and Z are the number of neutrons and protons and β is the deformation parameter for the complementary fragments 1 and 2. [β is defined in terms of the semimajor (c) and semiminor (a) axes of a prolate spheroid with $c = kr_0A^{1/3}(1 + 2\beta/3)$ and $a = kr_0A^{1/3}(1 - \frac{1}{3}\beta)$, where k is a volume conservation factor.] The liquid-drop energies (V_{LD}) and the shell (S) and pairing (P) corrections all include their dependence on deformation β. The dependence of the shell and pairing corrections on the intrinsic single-particle excitation τ is also indicated.

This approach implies a state of quasiequilibrium for the system near the scission point similar to that discussed by Nörenberg.[8] A condition of intermediate coupling is assumed between the collective and single-particle levels populated as the system moves along the fission degree of freedom toward scission. We describe this situation by introducing a collective temperature, T_{coll}, which characterizes the quasistatistical equilibrium of the collective degrees of freedom and a parameter, τ_{int}, an effective intrinsic temperature which determines the population of single-particle levels. In the extreme of strong coupling between collective and single-particle levels (the statistical model[7]), a statistical equilibrium is assumed among all degrees of freedom and a single temperature describes this state. The opposite extreme of zero coupling between collective and single-particle motion leads to the adiabatic model for spontaneous fission, with essentially all of the energy in collective degrees of freedom and none in single-particle excitation (i.e., $\tau_{\mathrm{int}} = 0$). The actual fission process probably lies somewhere between these extremes, with the nucleus exhibiting some coupling between collective and single-particle degrees of freedom, i.e., some viscosity.

The condition of intermediate coupling implies a finite value for τ_{int} even for spontaneous fission. In general, as the excitation energy of fission is increased, most of the additional energy above the fission barrier should contribute to intrinsic excitations and increase the value of τ_{int}. For convenience, we have chosen $\tau_{\mathrm{int}} = 0.75$ MeV and treated it as a constant for all fissioning systems.

Justification for this choice of τ_{int} will be given below. The Coulomb and nuclear interaction between the two fragments are given by V_C and V_n, respectively.

The assumption of a quasiequilibrium among collective degrees of freedom near the scission point is fundamental for the calculation of the relative probabilities of formation (fission yields) of complementary fission fragment pairs. The coupling among collective degrees of freedom is expected to be strong compared with that between collective and single-particle degrees of freedom as discussed by Nörenberg.[8] The statistical equilibrium among collective states can be characterized by a collective temperature T_{coll}, and the relative probability of formation of any fission fragment pair is then given by

$$P(N, Z, \tau, d) = \int_{\beta_1=0}^{\beta_{max}} \int_{\beta_2=0}^{\beta_{max}} \exp[-V(N, Z, \beta, \tau, d)/T_{coll}]\, d\beta_1 d\beta_2 , \tag{2}$$

where $V(N, Z, \beta, \tau, d)$ is the value of the potential calculated from Eq. (1). This is the basic equation in our model for the calculation of all distributions in mass, charge, kinetic energy, etc. The various distributions are calculated by summing over all deformation space and appropriate (N, Z) combinations. The integrations in Eq. (2) were terminated at $\beta_{max} = 1.0$ since the single-particle level calculation was limited to a basis set of 14 oscillator shells and large inaccuracies in the shell correction would be encountered for larger values of β. The value of T_{coll} was taken to be a constant (= 1.0 MeV) for all systems studied. The choice of this value is discussed below.

A. Collective parameters

Most of the energy of the system is contained in the liquid-drop terms V_{LD}. Fortunately, the various terms of the liquid-drop model are reasonably well known and their dependence on deformation can be calculated analytically. We have investigated both the liquid-drop model[14] and the droplet model[15] using the parameter values of Ludwig *et al.*[16] and have found no significant differences in the calculated total potential energy. The potential energy calculation at the scission point is sensitive principally to small changes in the values of N, Z, and β in the two spheroids. Both the liquid-drop and the droplet model vary quite smoothly with changes in N, Z, and β, thus minimizing the importance of any higher order terms.

The formula for the binding energy of a spherical nucleus without shell and pairing corrections is given by Seeger and Perisho[14] as

$$\begin{aligned} B(N, Z) = {} & 15.762A - 30.088I^2/A \\ & - 20.067A^{2/3} + 47.883I^2/A^{4/3} \\ & - \frac{0.864Z^2}{1.1927A^{1/3}} \left(1 - \frac{0.76361}{Z^{2/3}} - \frac{2.453}{1.1927^2 A^{2/3}}\right) \\ & + 7\exp(-6|I|/A) + 14.33\times 10^{-6} Z^{2.39} , \end{aligned} \tag{3}$$

where $A = N + Z$ and $I = N - Z$. The dependence of the various terms on deformation can be formulated in terms of the eccentricity of the spheroid and calculated analytically. These terms are conveniently tabulated by Hasse.[17]

The mutual Coulomb interaction V_C of two spheroids of charge $Z_1 e$ and $Z_2 e$ is given by

$$V_C = \frac{Z_1 Z_2 e^2 F}{D} , \tag{4}$$

where F (≈ 1.0–1.1) is a shape factor[18] representing the difference between the Coulomb interaction of two uniformly charged spheroids and that of two point charges separated by a distance D.

Krappe and Nix[19] have suggested a modification to the surface energy term in the liquid-drop formula. It is known that the deformation energy of strongly necked-in configurations show anomalously strong dependence on the exact details of the shape in the neck region. One of the special configurations they consider is that of two nonoverlapping spheres of radii R_1 and R_2 with a center of mass distance $D \geq R_1 + R_2$. They found the nuclear interaction energy between the two spheres for this configuration is

$$\begin{aligned} V_n = {} & -4\left(\frac{a}{r_0}\right)^2 a_s(1 - K_s I^2)\left(\frac{R_1}{a}\cosh\frac{R_1}{a} - \sinh\frac{R_1}{a}\right) \\ & \times \left(\frac{R_2}{a}\cosh\frac{R_2}{a} - \sinh\frac{R_2}{a}\right)\frac{e^{-D/a}}{D/a} , \end{aligned} \tag{5}$$

where a (= 1.4 fm), a_s (= 24.7 MeV), and K_s (= 4.0) are parameters determined by Krappe and Nix[19] from a fit to interaction barrier heights and fission barrier heights and r_0 is taken as 1.16 fm.

For the configuration of two nearly tangent spheroids, we approximate the nuclear interaction by replacing the radii of curvature in the above expression by the appropriate R_1 and R_2 radii of curvature of the two spheroids at the point of closest approach. Although such an approximation for

the neck region underestimates the nuclear interaction term in an absolute sense, it should reproduce fairly accurately the dependence on the separation distance between the two spheroids and exhibit the correct dependence on small changes in N, Z, and β.

Minimization of the potential energy of two spheroids connected by a neck would result in the unrealistic solution of two spheres at infinity connected by an infinitesimal neck (i.e., $V_n = 0$). A reasonable constraint on the calculation involves a limitation of the nuclear interaction V_n at the scission point to be the order of the binding energy of a nucleon. For a typical mass split and nucleon binding energy, this corresponds to a separation distance d between the tips of the spheroids of about 1.4 fm at the scission-point configuration. For simplicity in our calculation, we use this value of d for all fissioning systems.

It is interesting to note that the dependence of the Coulomb and nuclear interaction terms on the separation distance d produces a region of relatively constant potential energy over the range $0 \lesssim d \lesssim 2$ fm. There has even been a suggestion that a "scission barrier" may be present in this region.[8] Moreover, the presence of a nuclear viscosity (consistent with the value of $\tau_{\text{int}} \approx 0.75$ MeV) could slow the collective motion from saddle to scission. Thus, the time necessary for the establishment of a quasiequilibrium in the passage through the scission point may indeed exist, and our assumption of a statistical equilibrium among collective degrees of freedom at $d \approx 1.4$ fm as the basis for our calculation [Eq. (2)] is a reasonable one.

An estimate of the appropriate collective temperature T_{coll} to be used in Eq. (2) for the calculation of fission yields may be determined from charge dispersion data. The liquid-drop terms in Eq. (1) show a parabolic dependence in potential energy for a given mass split as a function of the nuclear charge Z with a minimum at the most probable charge Z_p. The shell and pairing terms can be neglected in the present context of establishing an overall, average estimate applicable to all mass splits, since they are generally small and roughly sum to zero when averaged over all N, Z, and β space. The equation of the parabola $V = \alpha(Z_p - Z)^2$ gives a value for α of ~1.53 MeV using the liquid-drop constants of Ludwig *et al.*,[16] a value of ~1.51 MeV using the constants of Seeger and Perisho[14] and a value of ~1.72 MeV using the constants of Myers and Swiatecki.[20] Charge dispersion data indicate a roughly Gaussian distribution with an average width of $\sigma = 0.56 \pm 0.06$.[21] Thus, one can equate the probability of formation and the charge dispersion Gaussian, or

$$e^{-V/T_{\text{coll}}} = e^{-\alpha(Z_p - Z)^2/T} = e^{-(Z_p - Z)^2/2\sigma^2} . \quad (6)$$

Then, solving for T, one obtains values of 0.96 MeV for $\alpha = 1.53$ MeV, 0.95 for $\alpha = 1.51$, and 1.07 for $\alpha = 1.72$. We have chosen an average value of $T = 1.00$ MeV for our calculation and treated it as a constant for all mass splits and fissioning systems studied.

Considerations of Q values and average total kinetic energies observed in the fission of various systems and our choice of $T_{\text{coll}} = 1.0$ MeV lead to an estimate for the average total intrinsic excitation energy of 10–20 MeV. Although this value is only poorly known, we have again chosen to simplify the calculation by choosing a representative value for the temperature corresponding to this energy range (i.e., $\tau_{\text{int}} = 0.75$ MeV) and taking it as a constant for all mass splits and fissioning systems. The sensitivity of the results of the calculation to the values of the parameters d, T_{coll}, and τ_{int} will be discussed below.

B. Shell corrections

The shell corrections can be easily calculated with the Strutinski prescription[1] once the single-particle levels have been generated. We have chosen for this purpose a Woods-Saxon potential. The potential parameters were[22]

$$r_0 = 1.265 \text{ fm}, \quad a = 0.659 \text{ fm},$$

$$V_n = 52.5 - 48.7\delta, \quad V_p = 52.5 + 48.7\delta ,$$

where $\delta = [(N - Z)/Z + 0.0112Z^2/A^{5/3}]/(1 + 3.5/A^{1/3})$. The strength function λ in the spin-orbit term was set at $\lambda = 38$ to reproduce the known level splittings in the mass region of interest. The use of a finite potential well requires that the lower quasistationary unbound states be included because the number of bound states are insufficient to carry out the appropriate averaging in the Strutinski prescription. The shell corrections were obtained using an eighth-order Hermite polynomial with a smearing width $\gamma = 8$ MeV. The shape deformations were introduced into the potential via the substitution,[23]

$$r^2 \rightarrow r^2[\cos^2\theta e^{-4\epsilon_2/3} + \sin^2\theta e^{+2\epsilon_2/3}] . \quad (7)$$

No higher order deformation terms, e.g., ϵ_3, $\epsilon_4, \ldots$, have been included in the calculation reported here. At the largest deformations investigated ($\epsilon_2 \sim 1.0$), the calculated shell corrections begin to show sensitivity to inclusion of one additional shell to the basis function set used to generate the single-particle levels. The shell corrections at the largest deformations are thus more uncertain. (It should be noted that the deformation parameter ϵ used here differs slightly from the β used elsewhere in this paper and the differ-

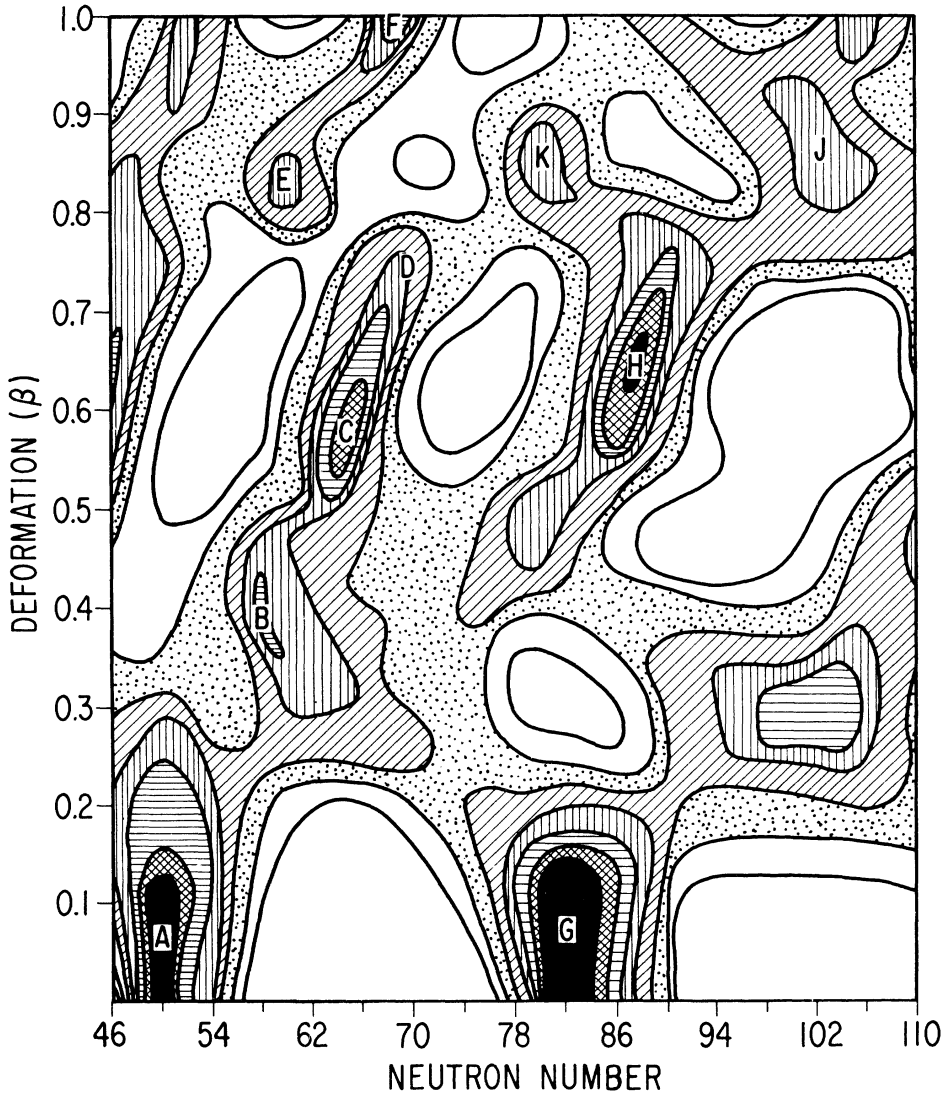

FIG. 1. Neutron-shell corrections calculated as a function of deformation (β) and neutron number. The contours are plotted at 1 MeV intervals with the black regions (representing the strongest shell corrections) containing all values lower than -4 MeV and the inner white region (representing the weakest shell corrections) containing all values greater than +2 MeV. The contours do not include any pairing or liquid-drop terms. The letters refer to particular shell regions as described in the text.

ence has been corrected for.)

The shell corrections calculated as outlined above are given in Figs. 1 and 2 for neutrons and protons, respectively. The contours indicate deep, spherical shell corrections at nucleon numbers 50 and 82 and "valleys" with local, relative minima (designated by letters) extending to large deformations between the spherical closed shells. The lettered regions will be referred to extensively in later discussions. The general features of these contours are common to all calculations using the Strutinski prescription.[1] There are, of course, differences in the detailed structure of the potential energy surface depending on the specific parameters used. A comparison of our results at the appropriate deformations with the experimental ground-state masses indicates a reasonable agreement over the entire region of interest except in the vicinity of the doubly-magic nucleus $^{132}_{50}$Sn. It is expected that the problem here is similar to the discrepancy in the ^{208}Pb region discussed extensively by Brack *et al.*[24] Using a Woods-Saxon potential, they found the calculated shell correction at the doubly-magic ^{208}Pb was overestimated by 5 MeV. Away from the doubly-magic region the Woods-Saxon potential gives

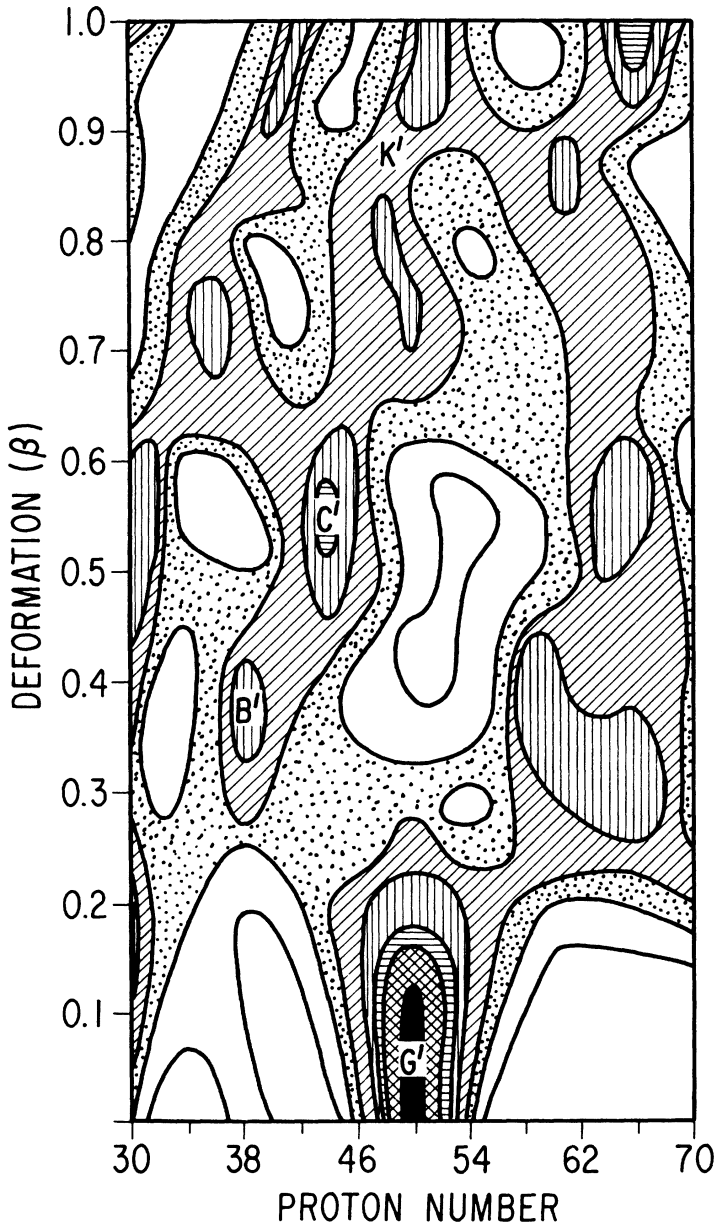

FIG. 2. Proton-shell corrections calculated as a function of deformation (β) and proton number. Other notations are the same as in Fig. 1.

very reasonable results for the shell corrections. We find the Strutinski procedure using Woods-Saxon levels yields a shell correction of 14 MeV for ^{132}Sn, whereas ground-state mass systematics would indicate a value in the vicinity of about 11.5 MeV.[25] The calculated value of the shell correction has been corrected to the experimental value in the region $N = 82$, $Z = 50$ and $0 \lesssim \beta \lesssim 0.1$. For all other values of (N, Z, β) space, the calculated values of the shell correction are used.

In much of the later discussion, the qualitative trends of the minima in the potential energy surface and the regions of deformation associated with them will be related directly to the qualitative trends in observed fission phenomena.

The nuclear shell effects calculated with the Strutinski method apply only to zero excitation energy. One can, in principle, calculate the shell effects as a function of excitation energy in the manner of Jensen and Damgaard.[26] For simplicity, we use the approximation described by them which reproduces their more exact calculations

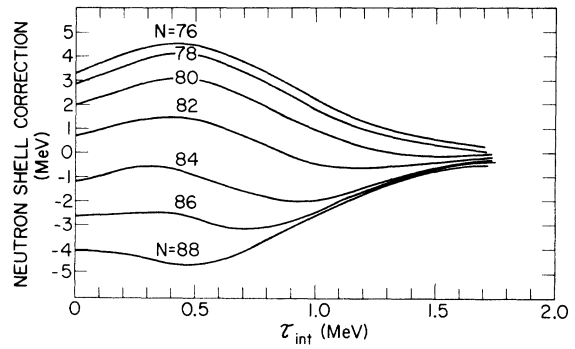

FIG. 3. The neutron-shell corrections at a fixed deformation ($\beta = 0.65$) calculated as a function of the intrinsic temperature, τ_{int}. These shell corrections correspond to those in the vicinity of point H of Fig. 1.

quite well. In this model the level density is written as

$$g(\epsilon) = g_0 + f \cos\left[\frac{2\pi(\epsilon - \epsilon_0)}{\hbar\omega_{sh}}\right], \tag{8}$$

where g_0 is the average single-particle level density, $\hbar\omega_{sh}$ is the shell spacing in the single-particle spectrum, ϵ_0 is the energy midway between two shells, and f is a strength parameter. The intrinsic temperature τ_{int} is defined in terms of a variable θ, and the temperature dependence of the shell correction at a given deformation β and nucleon number N is expressed as follows:

$$\Delta E_{\beta,N}(\theta) = -\left(\frac{\hbar\omega_{sh}}{2\pi}\right)^2 \frac{f\theta^2}{\sinh^2\theta} \times \left[\cos(2\pi y)\cosh\theta + \frac{f}{2g_0}\sin^2(2\pi y)\right], \tag{9}$$

where θ and y are defined along with other pertinent equations in Ref. 27. The values for $\hbar\omega_{sh}$, f, and g_0 for any particular deformation β and nucleon number N can be determined from the single-particle level density spectrum and the appropriate shell corrections at zero excitation energy.

The energy dependence of the neutron-shell correction in the region $N = 76-88$ and $\beta = 0.65$ is shown in Fig. 3. As pointed out by Jensen and Damgaard,[26] the figure illustrates that the maximum shell strength need not occur at zero excitation energy.

C. Pairing corrections

The pairing energy E_p is calculated using the standard BCS formalism[28] with the average pairing gap $\bar{\Delta} = 11/\sqrt{A}$ MeV for both neutrons and protons at zero temperature. The dependence of the average gap parameter $\bar{\Delta}$ on temperature has been calculated by Moretto.[29] He has shown that the average value of Δ deviates appreciably from the most probable value at temperatures near the critical temperature. We have approximated this temperature dependence by the following expression

$$\bar{\Delta}(\tau) = f(\tau)\bar{\Delta}, \tag{10}$$

where $f(\tau)$ is a polynomial fit to the results of Moretto. The pairing strength was assumed to be independent of surface area (i.e., deformation).[22]

III. MASS DISTRIBUTIONS

A. General discussion

Before discussing the detailed results of the calculation, it would be appropriate to make some general comments. We want to emphasize that our principle aim is to investigate the general validity and applicability of our model and not at this stage in its development to attempt to achieve the optimum fit to the experimental data for each fissioning system. We have thus chosen to use a constant set of values for the three parameters d, τ_{int}, and T_{coll} for all fissioning systems in order to reduce the computational chores. This simplification could lead to some difficulties, especially in the case of τ_{int}. In addition to expected differences in τ_{int} for the two readily available types of experimental fission data (spontaneous and neutron induced) with which the calculation will be compared, τ_{int} may also vary with the Z^2/A (i.e., the "fissility") of the fissioning system. Furthermore, we have used a single value for each of the three parameters, whereas it is to be expected that some dispersion around an average value would be a more realistic approximation. Thus, a consistent underestimate of the variance of any calculated distribution is expected.

Although a complete calculation [Eq. (2)] must be carried out to determine any particular distribution in fragment mass, charge, etc., much information on the observed trends and general features of the fission process can be obtained from an understanding of the influence of the deformed fragment shells alone. In the following discussions the complete calculation for representative systems will be presented and will be used as the basis for a qualitative, overall view of fission in terms of the fragment shell structure.

It may be helpful in achieving some perspective and in following the later discussion of the results in terms of the fragment shells to first examine the effects of the various terms contributing to the potential energy and to point out some general fea-

tures of the calculation. The liquid-drop contribution can be calculated with the shell and pairing corrections of Eq. (1) set to zero. Such a calculation for the potential energy as a function of deformation (β_1 and β_2) for a symmetric mass split in ^{236}U fission is shown in Fig. 4. A broad minimum in the potential energy (indicated by an X) occurs at $\beta_1 = \beta_2 \simeq 0.6$. These large fragment deformations at the potential energy minimum are the result of the Coulomb interaction [V_C in Eq. (1)] between the two fragments. The position of this minimum changes little for asymmetric mass splits, only becoming less deep as the asymmetry increases. The formation probabilities can be readily calculated from Eq. (2) and yield the symmetric mass distribution expected from liquid-drop considerations alone.[31] The liquid-drop behavior is similar for all fissioning systems, with only the position of the minimum changing smoothly and slowly to higher values of β as the charge and mass of the system increase.

Two points should be especially noted. First, shell corrections in the vicinity of the broad, liquid-drop minimum (at $\beta \approx 0.6$) will influence the probability of formation much more strongly than shells of equal strength located at deformations far from this minimum. Second, a spherical configuration for one fragment can be achieved only at considerable cost in liquid-drop energy and only be partially compensated by a large deformation in the complementary fragment.

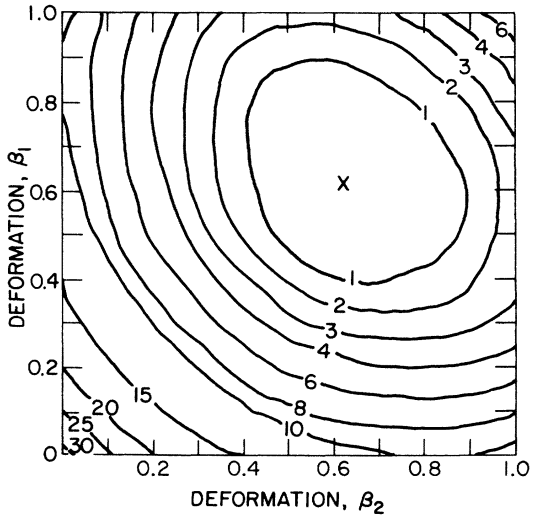

FIG. 4. A contour plot of the potential energy surface [Eq. (1)] for a symmetric mass split of ^{236}U calculated with the shell and pairing corrections set to zero. The symbol X marks the position, in deformation space, of the minimum potential energy. The numbers refer to the energy contours, in MeV, relative to the minimum potential energy at point X.

The microscopic corrections to the potential energy [Eq. (1)] include both shell and pairing terms. The pairing corrections are small compared to the shell corrections and are generally out of phase with them. This opposing behavior is understood in terms of the dependence of these correction terms on the density of single-particle states near the Fermi level. Owing to its relatively small magnitude, the pairing correction does not affect the position of the major shells or antishells significantly. Thus, a good qualitative picture of the major effects of the microscopic corrections can be obtained from an examination of the shell correction alone. In our model, this consists of a neutron and proton term for each of the two fragments. In fact, at the N/Z ratios appropriate for fission fragments, the major contribution to the shell correction for any particular mass split is generally that of the neutron shells. Thus, the overall trends in the microscopic correction terms can be most easily followed and understood in terms of the behavior of the neutron shells alone. We shall make use of this simplification in examining the results and predictions of the model later.

The influence of the shell-correction terms in the total potential energy calculation [Eq. (1)] may be illustrated for the case of a 140/96 mass split in ^{236}U fission. The liquid-drop contribution to the potential energy surface is much the same as that shown in Fig. 4. Addition of the shell-correction terms changes the surface markedly as shown in Fig. 5. Similar potential energy contours are shown in Figs. 6 and 7 for 134/102 and

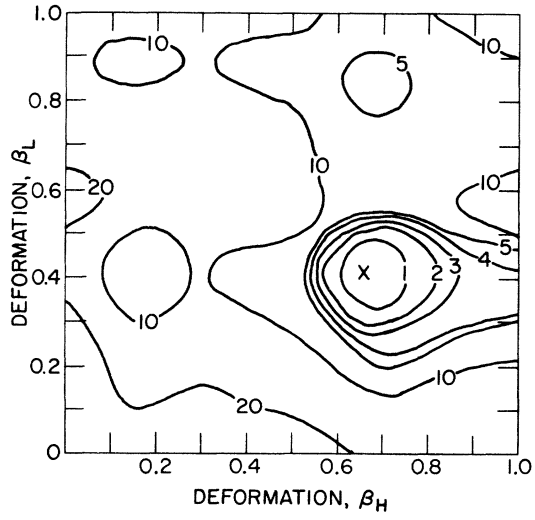

FIG. 5. A contour plot of the potential energy surface [Eq. (1)] for the 140/96 mass split in the fission of ^{236}U calculated with the shell and pairing corrections included. Other notations are the same as in Fig. 4.

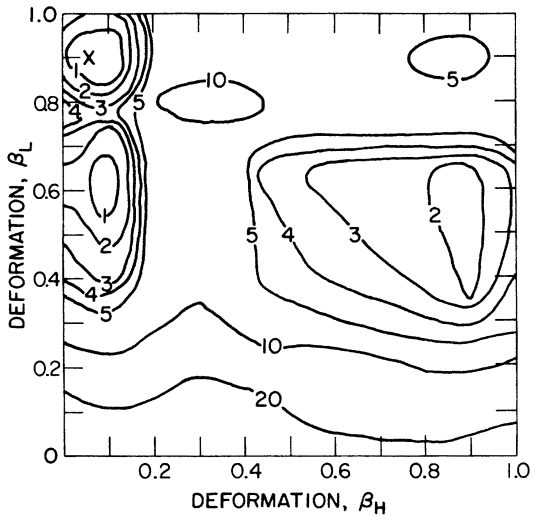

FIG. 6. A contour plot of the potential energy surface [Eq. (1)] for the 134/102 mass split in the fission of ^{236}U calculated with the shell and pairing corrections included. Other notations are the same as in Fig. 4.

118/118 mass splits, respectively. The potential energy minima (denoted by an X) in these figures can be readily associated with the shell structure at the appropriate deformations (β) shown in Fig. 1. Thus, in Fig. 5 the X corresponds to the neutron shells in Fig. 1 at points B and H, and in Fig. 6 it corresponds to the regions near points E and G. The symmetric mass split of Fig. 7 indicates two nearly equal minimum potential energy configurations denoted by X and Y. These do not correspond to a strong shell region in Fig. 1 as in the previous cases, but to a location to the right of point D with $N = 72$. The Y represents both fragments at $N = 72$, $\beta = 0.76$ and the X's represent one fragment at this position and the other at $N = 72$, $\beta = 0.52$.

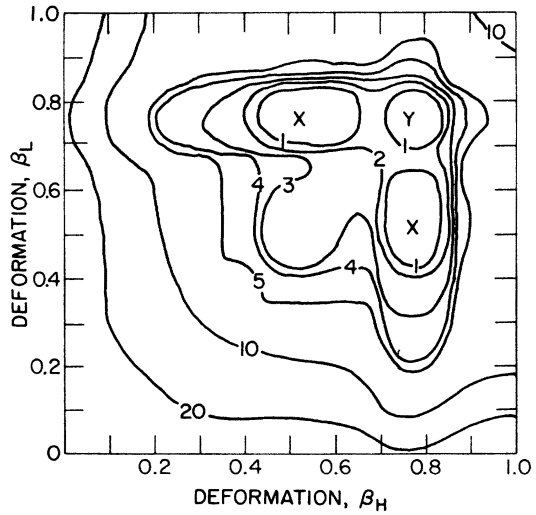

FIG. 7. A contour plot of the potential energy surface [Eq. (1)] for the symmetric (118/118) mass split in the fission of ^{236}U calculated with the shell and pairing corrections included. The symbols X and Y mark the positions of minima in deformation space of two configurations of nearly equal potential energy. Other notations are the same as in Fig. 4.

The mass yield for any mass split can be calculated from Eq. (2). The fragment deformations associated with the potential energy minima for each mass split correlate well with the well-known "saw-tooth" curve for neutron emission[30-32] which will be discussed later. In addition, the fragment deformations associated with a particular mass split (β_1 and β_2) enable one to estimate the distance between charge centers (D) and, hence, the total kinetic energy (TKE) for that split (i.e., TKE $= Z_1 Z_2 e^2/D$). It can be seen from the examples of Figs. 5–7 that the deformation for a symmetric mass split ($\beta_1 + \beta_2 \geq 1.30$) is significantly greater than for the 134/102 mass split ($\beta_1 + \beta_2 = 0.95$). This accounts for the well-known "dip" in TKE at symmetry for ^{236}U fission.[31] A similar model was used by Dickmann and Dietrich[9] in their calculation of TKE as a function of mass split for ^{236}U.

Calculations have been carried out for a wide range of fissioning systems (Po to Fm). The relative mass yields as calculated from Eq. (2) are shown in Fig. 8. These represent the primary

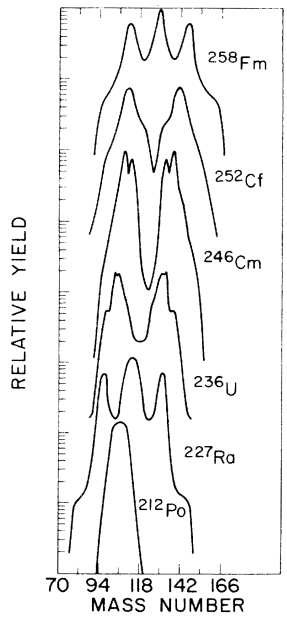

FIG. 8. Calculated mass-yield distributions for various fissioning systems using a single set of parameters ($T_{coll} = 1.0$ MeV, $\tau_{int} = 0.75$ MeV and $d = 1.4$ fm) for all systems.

fragment yields before neutron emission has taken place. The general trends which were so poorly understood for many years are well reproduced. From a narrow, symmetric mass distribution in the fission of nuclides in the region of Po the mass distribution becomes triple-peaked at Ra. It rapidly changes to an asymmetric distribution for nuclides from Th-Cf before once more favoring symmetry at ^{258}Fm. The nearly constant position of the heavy mass group and the shift in the light group position toward higher mass numbers as the mass of the fissioning nucleus increase are well-known phenomena[31] and are reproduced in the present calculation. As pointed out above, this systematic behavior is principally due to the deformed neutron shells and can be readily understood in terms of the fragment shell structure shown in Fig. 1.

In the case of ^{212}Po, the narrow, symmetric peak is a consequence of the strong neutron shell for a neutron number 64 at $\beta = 0.55$–0.60, indicated by C in Fig. 1. The potential energy minima for asymmetric splits lie along a "neutron channel" following the path B-C-D in Fig. 1. Away from the most favored symmetric configurations the yield drops due to a reduced shell strength and a less favorable liquid-drop energy. The total deformation remains nearly constant with mass split as a result of the nearly constant slope ($d\beta/dN$) of this neutron channel. A "proton channel" (path B′-C′ in Fig. 2) is in phase with the neutron-shell corrections in this case and enhances the effect of the latter.

Experimental data on the fission of Po are available only for excitation energies above about 40 MeV which are sufficiently high to reduce shell effects relative to liquid-drop effects. However, if experiments were performed at excitation energies of 30 MeV or less (e.g., using heavy-ion reactions with negative Q values) where shell effects would still predominate, our model predicts a narrow, symmetric mass distribution. The nuclides $^{192}_{76}$Os (with symmetric fragments of $Z_{1,2} \approx 38$ and $N_{1,2} \approx 58$) and $^{220}_{88}$Ra ($Z_{1,2} \approx 44$, $N_{1,2} \approx 66$) which have optimum shell strengths for both neutrons and protons should exhibit the narrowest, symmetric mass distributions at low excitation energies.

As the mass (and corresponding neutron number) of the fissioning system increases, the neutron-shell correction favoring symmetry rapidly decreases in strength beyond point D of Fig. 1 ($N \sim 70$, $\beta = 0.75$). Thus, for nuclides of total $N > 140$ a rapid inhibition of symmetric fission is expected and is observed experimentally. In the higher mass region ($N > 140$), the strong spherical neutron shell at $N = 82$ (point G, Fig. 1) and the deformed neutron shell at $N \approx 88$ (point H) become dominant and lead to asymmetric fission. The fact that the value of 1.0 MeV for T_{coll} is of the same order as (and, in particular, is not large compared with) the changes in shell strength per nucleon number enhances the rapidity with which particular shells can influence the relative probabilities for symmetric and asymmetric mass splits. This is evident from the exponential dependence on T_{coll} in Eq. (2).

The most prominent feature of nuclear fission in the actinides ($N_F > 140$) is the asymmetry of the mass split, with the heavy peak remaining essentially constant in position as the mass of the fissioning nucleus increases. This feature is accounted for by the influence of the strong neutron shell at point H (Fig. 1) with $N \approx 88$ and $\beta = 0.65$. The complement of this fragment will be at a deformation which lies along the neutron channel B-C-D discussed above in connection with the symmetric fission of ^{212}Po. Its position along the channel depends on its neutron number. Thus, as the mass of the fissioning system increases, the most probable mass split will be a heavy fragment of nearly constant neutron number and β close to point H with its light complement varying along the path B-C-D. Within a given system for mass splits more asymmetric than the most probable, the heavy fragment moves toward point J while the light fragment becomes less deformed, moving in the direction C-B-A. It may be noted here that these changes in deformation for the complementary fragments are consistent with the observations of the saw-tooth structure for neutron emission as a function of mass split in fission.[30-32] For example, in the case of ^{252}Cf the paths A-B-C-F for the light fragment and G-H-J for the heavy fragment closely follow the observed neutron emission pattern (Fig. 9). The energy available for neutron emission in each fragment is the difference in energy between the scission-point and ground-state shapes (E_{def}) plus any intrinsic excitation energy. Notice that at the deformation corresponding to the strong neutron shell at point H ($\beta = 0.65$) there is no strong proton shell ($52 < Z < 60$). The significance of this will be discussed later in connection with odd-even effects in the division of charge (cf. Sec. VI).

The complements of a spherical fragment with $N = 82$ are forced by liquid-drop considerations to become very deformed. The path E-F in Fig. 1 represents the locus of N and β for such fragments. Although a strong proton shell is present at $Z = 50$ (point G′, Fig. 2), its combination with $N = 82$ to give a "doubly-magic" $^{132}_{50}$Sn fragment is not particularly favored. The formation of such a fragment is hindered by a strong preference in the

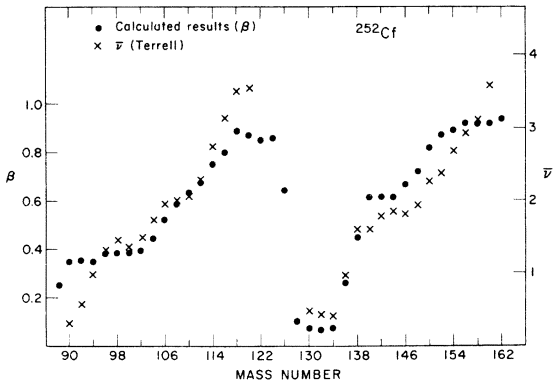

FIG. 9. The average deformation β of the fragments (symbol •) calculated for the fissioning system ^{252}Cf compared with the results of Terrell (Ref. 32) for $\bar{\nu}(A)$ in ^{252}Cf(sf) (symbol ×).

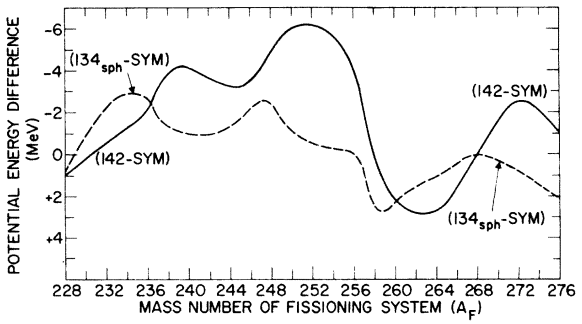

FIG. 10. The difference between the potential energy minima associated with two particular mass splits plotted as a function of the fissioning system A_F. The solid line represents the difference in energy between the mass split (142 + complement) and a mass symmetric split. The dashed line represents the difference in energy between a spherical mass 134 + complement and a mass symmetric split. The N/Z ratio for A_F was chosen to lie approximately along the valley of β stability for this calculation.

liquid-drop terms [Eq. (3)] for maintaining the N/Z ratio of the fragments close to that of the parent nucleus. To maintain the N/Z ratio of a typical actinide (e.g., $^{236}_{92}$U, $^{252}_{98}$Cf with ratios of ~1.57) an N of 82 would require $Z = 52$. The energy gained from the liquid-drop considerations (~6.5 MeV) more than compensates the loss in moving out of the $Z = 50$ shell to $Z = 52$ (~2.5 MeV) and a fragment of $A \sim 134$ is thus favored for $N = 82$. It should be noted that the total potential energy also involves consideration of the complementary fragment structure, but since these do not involve particularly strong shells along the path E-F they do not qualitatively affect the character of the mass split.

A surprisingly large number of the phenomena of fission, from general systematic trends to the detailed structure of various distributions in mass, kinetic energy, neutron emission, etc., can be accounted for rather simply in terms of the interplay of three basic configurations—a strong neutron shell at $N \approx 88$, $\beta = 0.65$ (point H of Fig. 1), the spherical neutron shell at $N = 82$ (point G), and the symmetric mass division favored by the liquid-drop terms in the potential energy calculation. A convenient presentation of this interplay is given in Fig. 10. Here the differences between the potential energy minima for two of these basic configurations and a symmetric mass split are plotted as a function of the mass of the fissioning system (A_F). The solid curve is the difference between the minimum potential energy for a mass 142 (effectively, the neutron shell at H in Fig. 1) plus its complement and the minimum potential energy for a symmetric mass split. The dashed curve is the difference between the minimum potential energy for a nearly spherical mass 134 (effectively, the neutron shell at G in Fig. 1) plus its complement and that for a symmetrical mass split. For the calculations of this figure, the N/Z ratio of A_F was chosen to lie approximately along the valley of β stability. In addition, it should be noted that the potential energies in this figure are calculated for $\tau_{int} = 0$.

Each curve in Fig. 10 is associated with a particular configuration for the heavy fragment. Thus the structure seen in the curves is, to first order, representative of the complementary light fragment configuration. For example, the peaks in the dashed curve at $A_F = 234$ and 247 are a consequence of the shell structure in the complementary light fragment at points E and F, respectively, in Fig. 1. This structure is reflected in prominent fission yield peaks for masses of the heavy fragment near $A_H = 134$ for these values of A_F and is observed as "fine structure" in the experimental mass yield distributions[33] for ^{235}U(n,f), ^{245}Cm(n,f), ^{246}Cm(sf), and ^{248}Cm(sf), where the complementary light fragments are $A_L = 102$, 112, 112, and 114, respectively.

In a similar way the peaks in the solid curve of Fig. 10 at $A_F = 239$ and 252 are associated with the light fragment shells at points B and C of Fig. 1. Large peak-to-valley ratios might be expected in the fission of species at these maxima. Before making a comparison with experimental data it is important to note that Figs. 8 and 10 refer to primary fragments and to a single value of τ_{int}. Experimental data represent the "secondary yields" of fission products after neutron emission from the fragments and must be corrected for comparison with the calculations. The yields at symmetry are particularly sensitive to the saw-tooth nature of the

neutron emission curve used in making this correction. Moreover, the peak-to-valley ratio varies rapidly with excitation energy (i.e., τ_{int}). The sensitivity of this ratio to the value of τ_{int} is illustrated in Fig. 11 which reproduces the well-known rise in the valley with increasing excitation energy in the case of ^{236}U fission. The effect is the result of the dependence of the shell strengths on excitation energy as shown in Fig. 3. At excitation energies where the shell corrections are reduced to zero, only the liquid-drop terms contribute to the potential energy calculation.

In general, the overall trends in mass distribution are easily seen in Fig. 10. Asymmetry is expected to predominate for $229 < A_F < 258$. Below $A_F = 229$ the shell stabilization for symmetric fission (the neutron valley along the path B-C-D of Fig. 1) rapidly increases, leading to the enhancement of symmetric fission. A proton shell (point C', Fig. 2) at $Z \approx 44, \beta = 0.55$ also begins to play an important part in the shell stabilization in this region of A_F. The combined effect of both a neutron and a proton shell can explain the very rapid shift in the character of the mass distributions observed for radium and thorium isotopes.

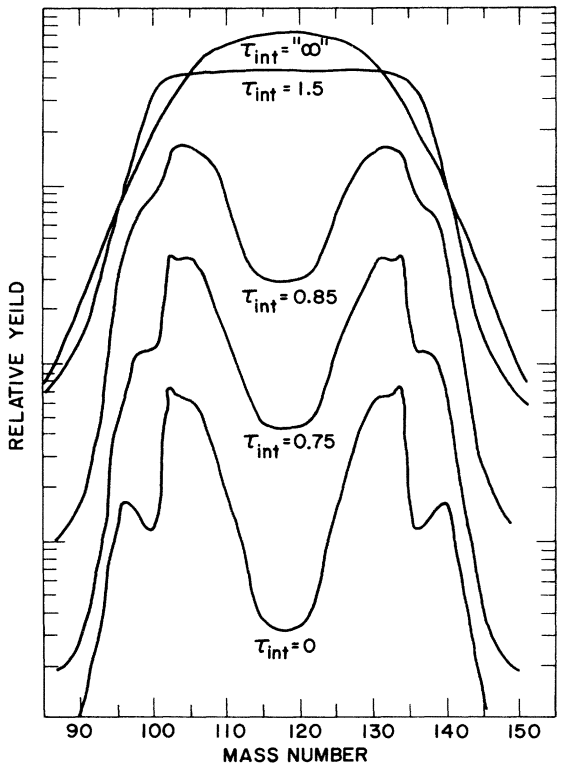

FIG. 11. The mass distribution for ^{236}U calculated at several different temperatures τ_{int}. The calculation at τ_{int} = "∞" has the shell and pairing corrections set to zero.

For $A_F \sim 258$ (and $N_F \sim 158$) another rapid variation in the character of the mass distribution is indicated in Fig. 10. The changes in this region can also be understood in terms of the fragment shell structures. At $A_F = 258$ the potential energy for an asymmetric mass split associated with points H and D of Fig. 1 is comparable to that for a symmetric mass split associated with points G and K. Asymmetry is favored for $A_F \lesssim 258$ and symmetry is favored for $A_F \gtrsim 258$. Note that the symmetric mass split has one spherical and one highly deformed fragment. This splitting is also enhanced by the presence of the strong, spherical proton shell at point G′ of Fig. 2 and the proton shell near point K′.

One might expect that two doubly-magic, spherical $^{132}_{50}$Sn fragments would represent the most probable division for the fission of $^{264}_{100}$Fm. Schmitt and Mosel[34] used a static scission model to calculate expected total kinetic energies for such configurations. However, in our model the shell stabilization is not sufficient to overcome the Coulomb repulsion for two nearly touching spheres. An increase in the neck distance d to values greater than ~2.5 fm is necessary before such a split becomes energetically favored. Addition of a dispersion in our chosen value of d might allow for a small contribution to the symmetric yield from such a doubly-spherical configuration.

The symmetric mass split with one spherical and one highly deformed fragment has a deformation $(\beta_1 + \beta_2 \sim 0.9)$ which is considerably less than that for the typical asymmetric split in Fm $(\beta_1 + \beta_2 \sim 1.40)$. Thus, a significantly higher total kinetic energy is expected for such a symmetric split and is in agreement with observations.[35] This configuration also implies a large variance in neutron emission for symmetric mass splits in the region of ^{258}Fm-^{264}Fm since the deformations of the mass symmetric fragments differ greatly. This is not the case for symmetric mass splits in other fissioning systems (e.g., in the Po-Ra region) where the fragments have similar deformations.

The probability of formation of mass splits around symmetry is expected to be most pronounced in the fission of ^{262}Fm and not ^{264}Fm since the neutron shell correction maximizes at $N_F = 162$ with $N_L = 80$, $\beta_L = 0.85$ and $N_H = 82$, $\beta_H \approx 0$. A maximum in the average total kinetic energy release ($\overline{\text{TKE}}$) of ~225 MeV and a minimum in the number of neutrons emitted per fission ($\bar{\nu}$) are also expected for ^{262}Fm since these average values are strongly affected by the high yields at symmetry. The high $\overline{\text{TKE}}$ is unique for this region and would not follow the systematic behavior observed for other systems as a function of $Z^2/A^{1/3}$.[36] The latter shows a monotonic increase in $\overline{\text{TKE}}$ with $Z^2/A^{1/3}$ which is simply a consequence of two op-

posing trends—the increase in the Coulomb interaction term and a slow increase in the separation of charge centers as indicated by an increase in a average total deformation $\langle \beta_1 + \beta_2 \rangle_{av}$. The narrow, symmetric mass distributions governed by shell effects (e.g., ^{192}Os, ^{220}Ra, and ^{262}Fm) should broaden as the shell corrections wash out with increasing excitation energy of fission and approach the symmetric mass distribution expected from liquid-drop considerations.

Although the mass distribution for any fissioning system can be calculated explicitly from our model, it is interesting and informative to extend the implications of the simple neutron-shell structure picture in Fig. 1 to give qualitative predictions of expected trends for systems beyond ^{264}Fm. The dominance of symmetry with the fragments near points G and K should continue until competition from asymmetric configurations involving points H and K is felt at $N_F \gtrsim 165$. The mass-yield curve in this region should be quite narrow with a small peak-to-valley ratio. Since the asymmetric scission configuration has a significantly larger total deformation than the symmetric one associated with the heavier fermium isotopes, the $\overline{\text{TKE}}$ should decrease accordingly. As additional nucleons are added to the fissioning system the most probable mass splits will comprise a heavy fragment at point H and its light complement moving along the path K-H. At $N_F = 176$ ($A_F \sim 284$) a very narrow, symmetric mass distribution is expected with both fragments at H. This configuration (in contrast with the ^{262}Fm case) is symmetric in deformation as well as mass and its total deformation ($\beta_1 + \beta_2 \simeq 1.30$) would imply a $\overline{\text{TKE}}$ consistent with the general systematics as a function of $Z^2/A^{1/3}$.[36] Above $A_F \simeq 284$, the mass distribution should become broader and more asymmetric with the light fragment now relatively fixed in position at H while the heavy fragment moves toward J. This trend should continue until the next major competition with shells at new configurations. Of course, in any specific case the effect of the proton shells, the contributions of other configurations, and, in fact, the complete calculation of the potential energy [Eq. (1)] is needed to evaluate the mass distribution. However, the simple qualitative approach utilizing Fig. 1, as outlined above, provides a useful perspective.

B. Detailed comparison with experimental data

Although the choice of a single parameter set ($T_{\text{coll}} = 1.0$ MeV, $\tau_{\text{int}} = 0.75$ MeV, and $d = 1.4$ fm) may not be optimum for all fissioning systems, it is of interest to compare our results with the experimental data in detail. Such a comparison provides a useful insight into the validity of the model and may suggest functional dependences of the parameters of our model on the Z^2/A and excitation energy (E^*) of the fissioning system.

Primary fission yield data for ^{252}Cf(sf) (Ref. 33), ^{235}U(n_{th},f) (Ref. 33), ^{226}Ra(p,f) (Ref. 38), and ^{257}Fm(n,f) (Ref. 35) are compared with our calculated mass distributions in Figs. 12–15, respectively. The general features of the data are well reproduced by our model. However, there are several quantitative discrepancies. The calculated distributions are too narrow and the positions of the asymmetric peaks are displaced somewhat—particularly for ^{235}U(n,f) and ^{226}Ra(p,f). In addition, the calculated peak-to-valley ratios for ^{236}U and ^{252}Cf are too small.

Apart from any inadequacies in our model and the neglect of dynamical effects or dispersions in the values of the parameters used, there are several possible sources of the discrepancies between the data and the calculations. Errors in the shell correction can arise in three ways: (1) errors in the parameters of the single-particle potential, (2) the neglect of higher-order multipole deformations in our calculation, and (3) errors arising from the Strutinski prescription for calculating shell corrections.

The agreement between our calculations and ex-

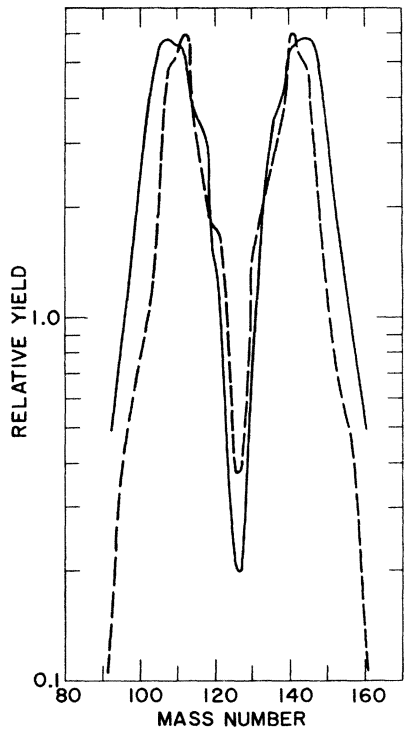

FIG. 12. Comparison of the calculated mass distribution for ^{252}Cf (dashed line) with the experimental data for ^{252}Cf(sf) (Ref. 33) (solid line).

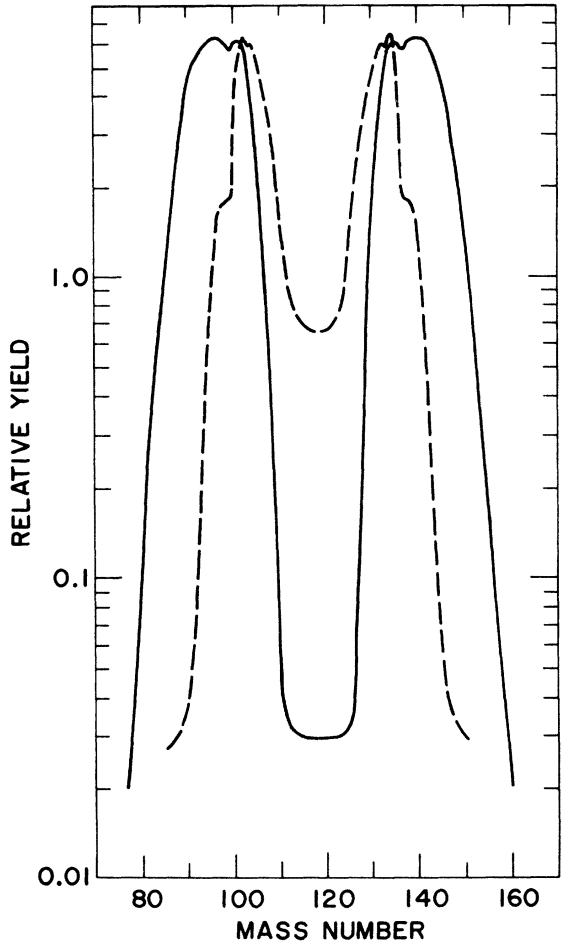

FIG. 13. Comparison of the calculated mass distribution for ^{236}U (dashed line) with the experimental data for ^{235}U(n_{th},f) (Ref. 37) (solid line).

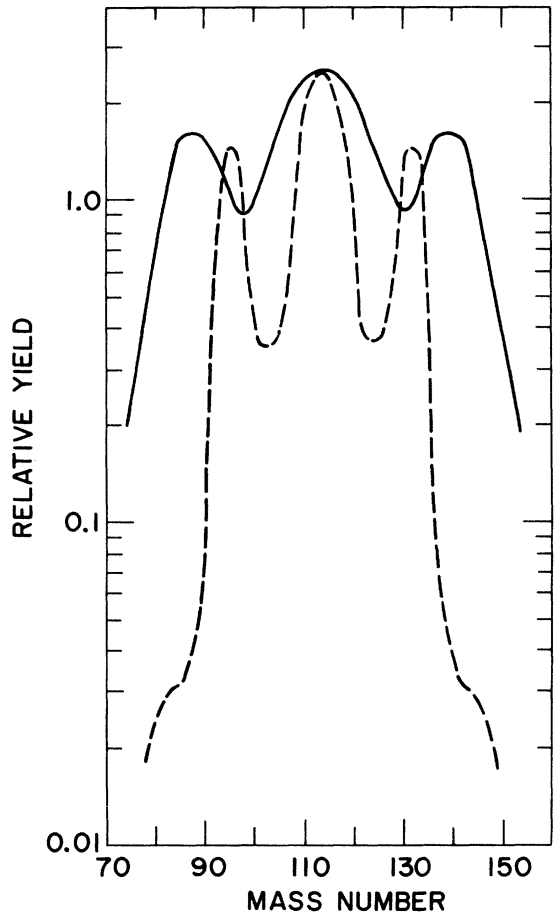

FIG. 14. Comparison of the calculated mass distribution for ^{227}Ra (dashed line) with the experimental data for ^{226}Ra(p,f) at $Ep = 13$ MeV (Ref. 38) (solid line).

perimental mass distributions is consistently improved for all systems by deepening the neutron-shell correction at $\beta \sim 0.3$ for the region of neutron numbers between ~54–68 in Fig. 1 and/or the proton-shell correction at the same β for proton numbers ~35-44 in Fig. 2. For the heavier actinides this region is associated with mass splits of low fission yield and the effect appears as a shoulder on the asymmetric wings of the calculated mass distributions at $A_L \approx 96$ (cf. Figs. 8, 12, and 13). In the range of fissioning nuclei from Ra to U, however, some of the most probable light fragments have deformations corresponding to this region. This leads to a prominent effect on the mass-yield curve in the asymmetric peak regions of ^{227}Ra at $A_L \leq 95$ and $A_H \geq 132$ (Fig. 14) and of ^{236}U at $A_L \leq 96$ and $A_H \geq 140$ (Fig. 13). An increase in the sum of neutron- and proton-shell corrections of ~1.5 MeV is sufficient to give good agreement between the calculated and experimental results. The shell correction method of Strutinski is not expected to be more accurate than ~0.5–1.0 MeV (Ref. 24) and, hence, a combined error of ~1.5 MeV for neutron and proton shells is quite plausible. The effect of such an error in the shell correction can also be seen in Fig. 10. For systems with $237 < A_F < 258$, the model correctly predicts a peak in the asymmetric mass yields near $A_H = 142$. However, for systems with $228 < A_F < 237$, the solid curve in Fig. 10 shows a rapid decrease below the dashed curve associated with $A_H = 134$. A broad maximum in the solid curve which maintains it above the dashed curve would result from the suggested shell-correction increase of ~1.5 MeV and raise the yield of fragments in the region of $A_H = 142$ relative to that at $A_H = 134$. This would bring the position of the peaks in the mass distributions of ^{235}U(n,f) and ^{226}Ra(p,f) in better agreement with experimental data.

Higher multipole-order deformations would lower the entire liquid-drop potential energy several

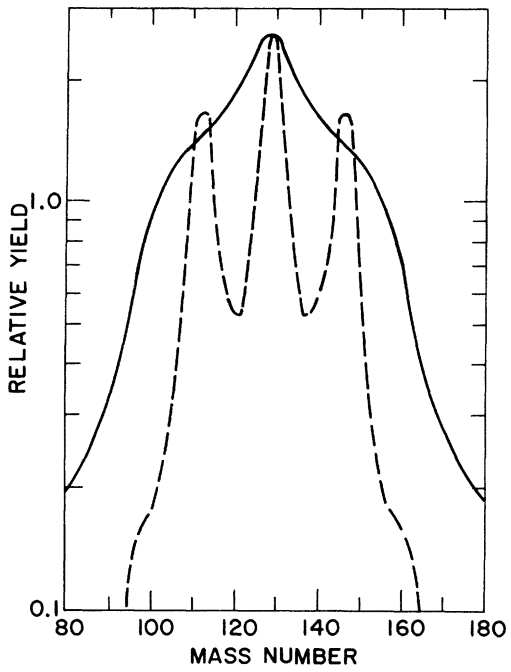

FIG. 15. Comparison of the calculated mass distribution for ^{258}Fm (dashed line) with the experimental data for ^{257}Fm(n_{th},f) (Ref. 35) (solid line).

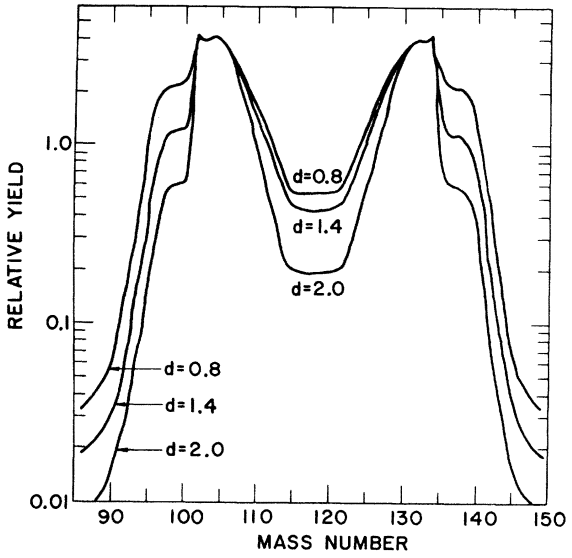

FIG. 16. The calculated mass distribution of ^{236}U for different values of d (the distance between the tips of the two spheroids) holding the value of the other parameters fixed (see text). The relative mass distributions have been normalized at mass 134.

MeV.[39] Moreover, they would perturb the shell corrections for particular single-particle levels, especially in the regions of high level density. The introduction of such deformations entails a large expansion of the calculational effort and has not yet been attempted.

Another possible source of error in our calculation arises from uncertainties in the parameters of the liquid-drop model at the large deformations associated with the scission point. Hasse[17] has investigated the dependence of mass asymmetry on various terms of the droplet model and noted especially the effect of the Coulomb redistribution term in this regard. Such dependences may be a cause of the insufficient widths of the calculated mass distributions.

The sensitivity of the calculation of mass distributions to the parameters d and T_{coll} are illustrated for the case of ^{236}U in Figs. 16 and 17, respectively. These parameters do affect both the widths and peak-to-valley ratios. Any change in d or T_{coll}, however, must also be compatible with its effect on TKE and charge dispersion. In general, the overall agreement of the calculated mass distributions with experimental data is not substantially improved by a change in the value of d or T_{coll}.

The parameter τ_{int} is expected to be an increasing function of the Z^2/A of the fissioning system as a result of the shape changes between the saddle and scission points. An increase in Z^2/A is associated with a greater difference between saddle-point and scission-point shapes.[18] The transition from saddle to scission would thus entail a larger number of level crossings for the higher Z systems, resulting in greater internal excitation due to frictional heating. It is also expected that τ_{int}

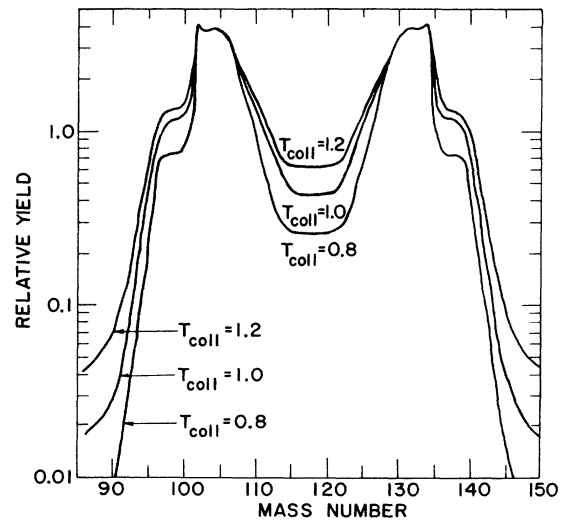

FIG. 17. The calculated mass distribution of ^{236}U for different values of the parameter, T_{coll}, holding the value of the other parameters fixed (see text). The relative mass distributions have been normalized at mass 134.

should be larger for reaction-induced fission than for spontaneous fission. The sensitivity of the calculated mass distribution to τ_{int} is illustrated in Fig. 11. The choice of τ_{int} =0.75 MeV gives a good fit to the peak-to-valley ratio for ^{252}Cf (Fig. 12). A smaller value for ^{236}U and a larger value for ^{257}Fm would help to remove the discrepancies between the calculations and experimental data in both systems, giving a larger peak-to-valley ratio in ^{236}U (Fig. 13) and raising the deep valleys in ^{257}Fm (Fig. 15).

In general, the discrepancies between the calculations of our model and experimental results are not large and have plausible explanations. It is, in fact, rather surprising and encouraging that one set of the parameters T_{coll}, τ_{int}, and d and a simple, static scission-point model yield such good results over so broad a range of fissioning systems. We hope to extend the calculations to include β_3 and β_4 deformations and to investigate the role of τ_{int} in more detail.

IV. KINETIC ENERGY DISTRIBUTIONS

A. General discussion

The total energy release at scission is given by

$$Q_{sciss} = V_C + E_{pre} + \sum_{1,2} E_{def} + \sum_{1,2} E_{int}\,, \tag{11}$$

where V_C is the Coulomb interaction energy at the scission point [Eq. (4)], E_{pre} is the prescission kinetic energy (i.e., the relative motion of the nascent fission fragments in the fission direction developed along the path between the saddle point and the scission point), and $\sum_{1,2} E_{def}$ and $\sum_{1,2} E_{int}$ are the sums of the energies contained in deformation and intrinsic excitation, respectively, of the two fragments at the scission point. Essentially all of V_C appears as relative motion of the fragments on separation (i.e., post-scission kinetic energy). A small fraction may appear as intrinsic excitation in the fragments. The post-scission KE may be approximated as $Z_1Z_2e^2/D$ since the shape factor F [Eq. (4)] and the fraction of V_C lost in excitation of the fragments are of about the same magnitude (a few percent) and tend to cancel. The deformation energy E_{def} is the energy required to deform each fragment from its ground-state shape to its shape at the scission point and can be calculated from the deformation dependence of the liquid-drop and shell- and pairing-correction terms of Eq. (1).

Two approximations for the total kinetic energy (TKE) of the fragments can be obtained from Eq. (11). In one, E_{pre} is assumed to be zero and TKE is then simply the post-scission contribution, i.e.,

$$\mathrm{TKE} \approx \frac{Z_1Z_2e^2}{D}\,. \tag{12}$$

In the other, $\sum_{1,2} E_{int}$ is assumed to be zero, and TKE is given by

$$\mathrm{TKE} \approx Q_{sciss} - \sum_{1,2} E_{def}\,. \tag{13}$$

The actual TKE is expected to lie between the two values. The difference between these two estimates for a particular configuration is equal to $(E_{pre}+\sum_{1,2} E_{int})$ and must be ≥ 0. The value of TKE for any mass split is obtained for each of the above estimates by the use of Eq. (2) with appropriate weighting over all deformation space and (N, Z) combinations.

Dickmann and Dietrich[9] have shown that the experimentally observed variation in kinetic energy as a function of mass split is reasonably well accounted for with the scission-point fragment shapes derived from a deformed-shell model. A dynamical calculation by Davies *et al.*[40] indicates that very extended scission shapes for the fragments are also consistent with the observed TKE data if a large prescission kinetic energy is present. Clearly, fitting of the TKE data alone is not sufficient to determine the scission-point configurations. The latter must also be consistent with other data such as the saw-tooth structure in the neutron-emission function and the mass and charge distributions of the fragments if these are determined near the scission point.

The most prominent structure in the experimental data on TKE as a function of mass split in the fission of actinide nuclei is the appearance of a "dip" at symmetry.[30,31,41] This is readily understood in terms of the shell structure of the fragments at scission. Figure 18 shows the variation of the value of the parameter $(\beta_1+\beta_2)$ as a function of A_F for two scission configurations—mass sym-

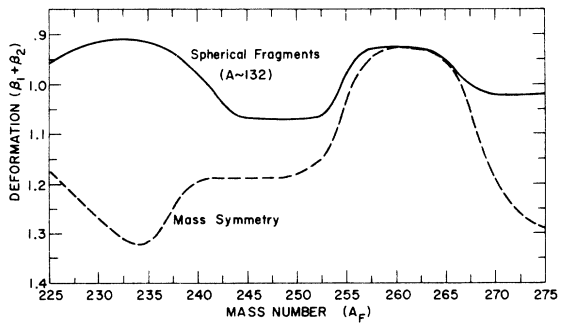

FIG. 18. The average total deformation coordinate $(\beta_1+\beta_2)$ plotted as a function of the fissioning system A_F for two different scission configurations—a spherical mass in the region of $A \sim 132$ plus its complement and mass symmetry.

metry and a division with one fragment spherical at $A \approx 132$. Note the inverted scale in the figure. The smaller the value of $(\beta_1 + \beta_2)$, the smaller the total distance between the fragments at scission and, hence, the larger the value of the TKE. The difference between the curves in Fig. 18 is proportional to the extent of the dip in TKE expected at symmetry. The largest difference is seen to occur in the region of $A_F \sim 235$ ($N_F \sim 144$), in agreement with the experimental data. This behavior can be understood in terms of the shell structure of Fig. 1. The spherical fragment of $A \sim 132$ ($N \sim 82$) is at point G while its complement ($N \sim 62$) is near point E at $\beta \sim 0.85$. For the symmetric mass split, one fragment is near point D at $\beta \sim 0.75$ and its complement is split between $\beta \sim 0.75$ and $\beta \sim 0.5$ with about equal probability, giving a much larger total deformation (cf. Fig. 7).

In the curium region ($A_F \sim 245$), the situation changes significantly. The complement of the spherical 132 fragment moves to larger deformations near point F in Fig. 1 while the mass symmetric split occurs with β values of 0.75 and 0.45, thus greatly reducing the extent of the dip in TKE expected at symmetry. Another significant change is expected in the region of the heavy fermium isotopes. The complement of the spherical $A \sim 132$ fragment at point G is now near symmetry and its shape is determined by the shell at point K. This configuration represents a small total deformation and leads to the prediction of a high value for TKE at symmetry and the disappearance of the dip. This has recently been observed experimentally.[35,42]

An interesting situation arises in the region of $A_F \sim 270$. Figure 18 indicates a difference in deformation appearing for the two configurations. However, this does not necessarily mean that a reduction in TKE is expected at symmetry in these systems. Each configuration must be weighted by its contribution to the fission yield. For systems of very high Z, the energy gain from the shell stabilization of the spherical 132 fragment is not sufficient to overcome the increased repulsion arising from the Coulomb interaction term and thus the spherical 132 does not contribute to a significant fraction of the yield for this mass split. The appropriate deformations of high yield are associated with points H and K (Fig. 1) and are comparable to those for mass symmetry. A consequence of this is the expected disappearance of the saw-tooth structure in the neutron-emission function which is due to the predominance of the strong spherical shell in the $A \sim 132$ region.

B. Detailed comparison with experimental data

Experimental data for total kinetic energy release as a function of fragment mass are shown in Figs. 19–21 for the systems ^{226}Ra(p,f),[38] ^{252}Cf(sf),[43] and ^{257}Fm(sf),[42] respectively. These data are compared with calculations from our model for the two estimates of TKE as described in the previous section. The calculation of TKE is particularly sensitive to the value of d, the distance between the spheroids. An increase in d reduces directly the value of TKE from Eq. (12). However, the value obtained from Eq. (13) may or may not be affected. The average deformation of the fragment at low excitation energy is determined by particular shells. Reducing the Coulomb interaction term (V_C) through an increase in d may or may not be sufficient to shift the potential energy minimum to a less deformed shape. If no shift occurs, this estimate of the TKE does not change appreciably with a change in d.

The calculations follow the general trend of the data quite well. The dips at symmetry and peaking at $A_H \sim 132$ for ^{227}Ra and ^{252}Cf fission are well reproduced. For ^{258}Fm, the calculated peak at $A_H \sim 132$ occurs near symmetry and reflects the

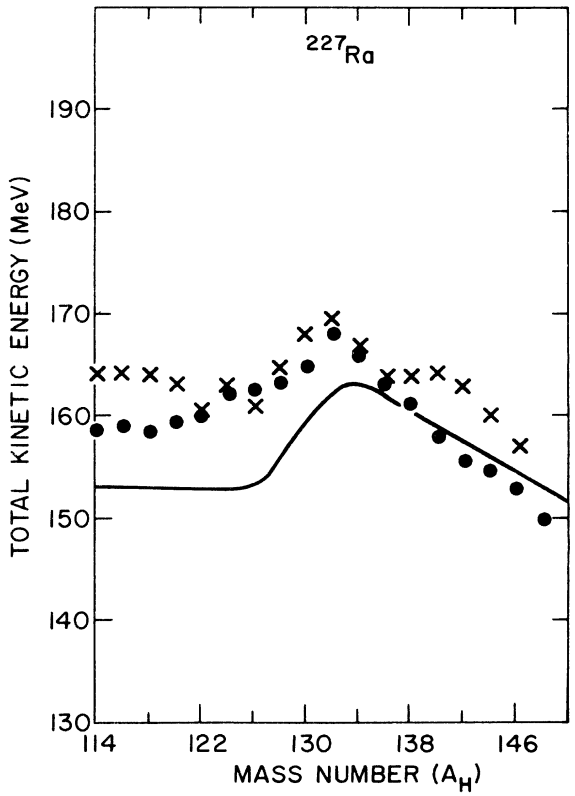

FIG. 19. Comparison of the calculated total kinetic energy (TKE) for ^{227}Ra with the experimental TKE for ^{226}Ra(p,f) at $E_p = 13$ MeV (Ref. 38). The solid line represents the experimental data while two estimates of the TKE from our model are represented by the symbols X (from $Q_{\text{sciss}} - \Sigma_{1,2} E_{\text{def}}$) and • (from $Z_1 Z_2 e^2/D$) as described in the text.

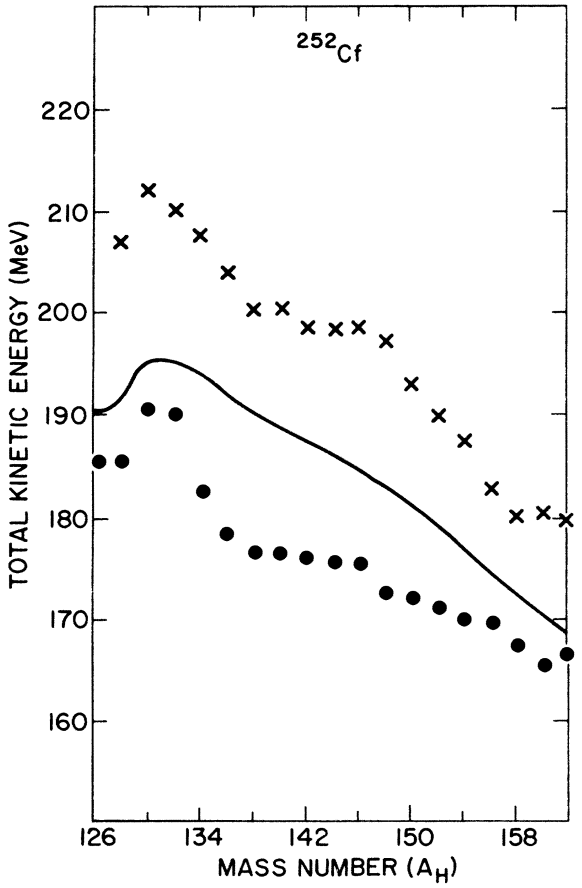

FIG. 20. Comparison of the calculated total kinetic energy (TKE) for ^{252}Cf with the experimental TKE for ^{252}Cf(sf) (Ref. 43). The solid line represents the experimental data while two estimates of the TKE from our model are represented by the symbols X (from $Q_{\text{sciss}} - \Sigma_{1,2} E_{\text{def}}$) and • (from $Z_1 Z_2 e^2/D$).

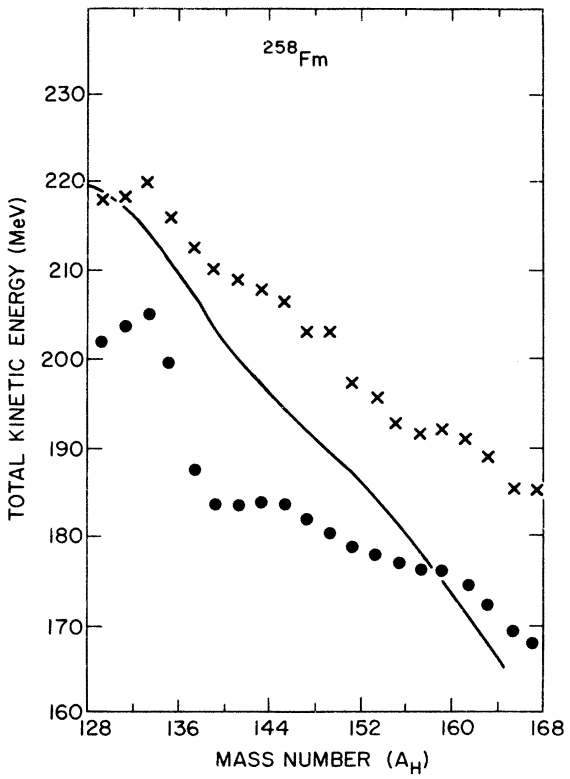

FIG. 21. Comparison of the calculated total kinetic energy (TKE) for ^{258}Fm with the experimental TKE for ^{257}Fm(sf) (Ref. 42). The solid line represents the experimental data while two estimates of the TKE from our model are represented by the symbols X (from $Q_{\text{sciss}} - \Sigma_{1,2} E_{\text{def}}$) and • (from $Z_1 Z_2 e^2/D$).

influence of the shells at G and K (Fig. 1). The calculation is in reasonably good agreement with experimental data for ^{257}Fm. Since the neutron-emission function for ^{257}Fm is not known, the correction of observed data to primary fragment masses and energies may lead to some uncertainty, particularly in the symmetric mass region. There is obviously a difficulty in the case of ^{227}Ra where the data lie below both TKE estimates. The TKE estimate of Eq. (12) could be reduced ~3.5%. by an increase in the value of d from 1.4 to 2.0 fm. Such a change removes the discrepancy without affecting the value calculated from Eq. (13) appreciably. The agreement between experimental and calculated mass distributions is not significantly affected by such a change (cf. Fig. 16).

A large body of experimental data has been accumulated on average total kinetic energy release ($\overline{\text{TKE}}$) for many fissioning systems. These data are heavily weighted by the contribution from the most probable mass splits. As discussed in the section on mass distributions, the most probable mass split for the fissile nuclei from Th-Cf is determined by the shell near point H (Fig. 1). For these systems the most probable heavy fragment remains fixed near $A_H = 142$. Systematic trends in $\overline{\text{TKE}}$, then, should reflect the most probable deformations of the complementary light fragments.

In Fig. 22 we plot the sum of the neutron- and proton-shell corrections of the fragments complementary to 142 [i.e., $(A_F - 142)$] as a function of the fissioning system A_F. The N/Z ratio of A_F is chosen along the valley of β stability. For convenience, scales for $(A_F - 142)$ and N_L are also given. The open circles mark the deformations associated with the calculated minimum potential energy for the most probable light fragments. The addition of neutrons to the light fragment does not change the deformation appreciably over the range $234 \lesssim A_F \lesssim 244$. Since the heavy fragment is fixed at point H (Fig. 1), the $\overline{\text{TKE}}$ for these sys-

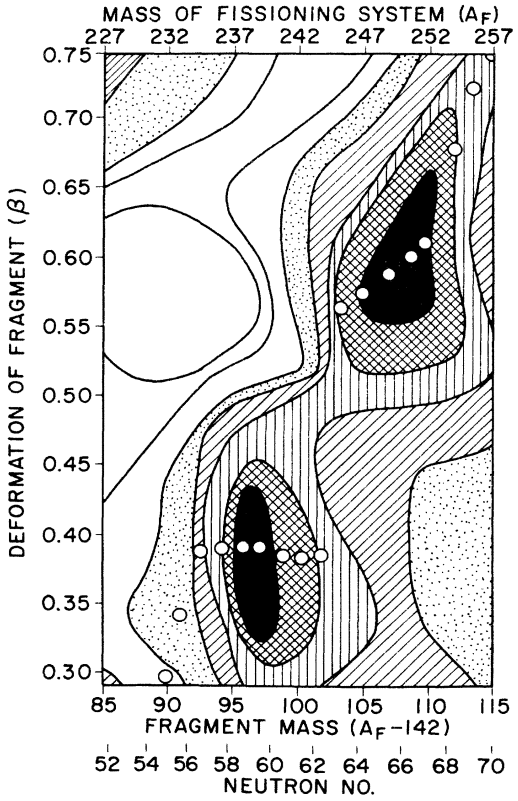

FIG. 22. The sum of the neutron- and proton-shell corrections at different deformations β, for the light fragment complementary to mass 142 at $\beta_H = 0.65$. For convenience, the mass of the fissioning system (A_F), the mass of the light fragment ($A_F - 142$), and the neutron number of the light fragment are all shown on the abscissa. The N/Z ratio for the fissioning system was chosen to lie approximately along the valley of β stability for this calculation. The open circles represent the deformation of the light fragment ($A_F - 142$) at its potential energy minimum for various fissioning systems.

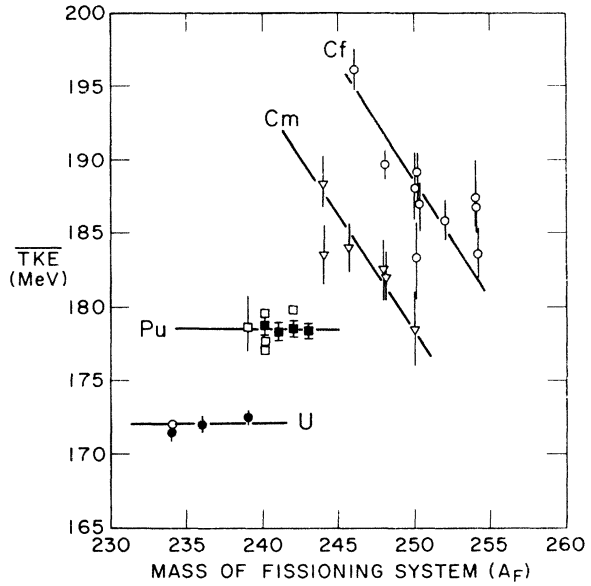

FIG. 23. The experimental results for $\overline{TKE}$ for the isotopes of U, Pu, Cm, and Cf as given by Vorob'eva *et al.* (Ref. 44).

tems should be independent of neutron number for a given Z_F. The situation changes abruptly, however, for $A_F \gtrsim 244$ ($N_F \gtrsim 149$). The average deformation of the most probable light fragment shifts rapidly to a different shell-correction minimum at greater deformation. The deformation of the light fragment increases further with the addition of neutrons to the light fragment so that a decrease in $\overline{TKE}$ is expected for isotopes of fissioning species in this region.

Experimental data on the isotopic dependence of $\overline{TKE}$ for U, Pu, Cm, and Cf fission have been published by Vorob'eva *et al.*[44] and are reproduced in Fig. 23. No interpretation of these results was proposed by the authors. However, the trends are precisely those suggested by the discussion of Fig. 22 above.

A general increase in $\overline{TKE}$ is expected as the nuclear charge of the fissioning system increases and has been shown by Viola and Sikkeland[36] to follow a linear $Z^2/A^{1/3}$ dependence. A deviation from this systematic behavior in the case of the spontaneous fission of Cm and Cf isotopes has been noted by Unik *et al.*[33] This is explained by an abrupt increase in the deformation of the light fragment at $A_F \sim 244$ (Fig. 22) which leads to the reduction in the magnitude of the Z dependence of $\overline{TKE}$ in this region. In the case of Fm isotopes, the yield of the mass-symmetric component (with the fragments near points G and K in Fig. 1) increases rapidly with neutron number. This configuration has a smaller total deformation and its contribution to $\overline{TKE}$ will cause the latter to increase with increasing neutron number for Fm isotopes of $A \gtrsim 256$.

Further evidence in support of the general pattern of the shell structure for the light fragment and its deformation dependence can be found in data on the average number of neutrons emitted per fission ($\bar{\nu}_T$) for different fissioning systems. The quantity $\bar{\nu}_T$ is weighted by fission yields and its dependence on the total deformation of the fragments is the inverse of that of the $\overline{TKE}$. Figure 24 shows data on $\bar{\nu}_T$ as a function of A_F.[33] The two relatively flat regions for $230 \lesssim A_F \lesssim 236$ and $246 \lesssim A_F \lesssim 256$ with a transition region between them correspond to the deformations associated with the open circles of Fig. 22. The transition in the deformations is seen to be quite sharp at

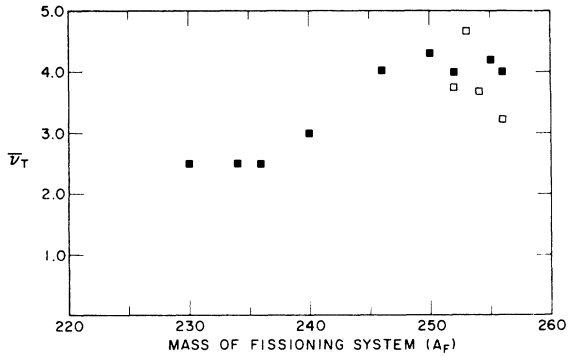

FIG. 24. The total average neutron emission $\bar{\nu}_T$ as a function of the mass of the fissioning nucleus as given by Unik *et al.* (Ref. 33). The solid squares represent data for neutron-induced fission and the open squares, spontaneous fission.

$A_F \approx 244$ ($N_F \approx 149$) in Fig. 22. However, the change in $\bar{\nu}_T$ for this mass region would not be as sharp owing to contributions from yields both lighter and heavier than the most probable. Again, the Fm isotopes will exhibit the effects of the high yields of the low-deformation, symmetric mass splits on $\bar{\nu}_T$.

The specific shell effects we have been discussing are dependent on excitation energy as illustrated, for example, in Fig. 3. Although a large body of data exists on the effect of excitation energy on $\overline{\text{TKE}}$, the averaging process complicates any resolution of the contributions of specific effects. The shell effects would be more readily observed in kinetic energy data for particular mass splits as a function of excitation energy and fissioning species. These effects will depend on such factors as the scission-point temperature, the deformation and "strength" associated with particular shells, the availability and competition of other shells at different deformations for the mass splits under consideration, and the preferred liquid-drop deformation.

As pointed out previously, Fig. 3 indicates that the excitation energy (E^*) dependence of the shell correction is complex and changes with the region of τ_{int}. For values of τ_{int} in the region of ~0.5 MeV, several MeV of additional E^* may result in no significant change in the shell corrections and, hence, no change in deformation or fission yield. For larger values of τ_{int} ($\gtrsim 0.7$ MeV) an increase in E^* leads to a diminution of the shell correction which is approximately proportional to the value of the correction. As E^* increases and the shell correction diminishes, the potential energy surface relaxes to that determined by the liquid-drop terms. The configuration of the fragments at the scission point changes accordingly from a total deformation $(\beta_1 + \beta_2)$ associated with the potential energy minimum resulting from the shell correction to that associated with the liquid-drop terms, with accompanying changes in $\overline{\text{TKE}}$, $\bar{\nu}$, etc. This change will take place rather slowly as the large shell correction diminishes with E^*. If, however, a secondary minimum in the surface is present at low E^* (associated with another shell) at a value of $(\beta_1 + \beta_2)$ close to that of the liquid-drop value, its relative contribution to the fission yield for the mass split involved will increase quite rapidly with increasing E^* for $\tau \gtrsim 0.7$. The rate at which this occurs should be related to the difference in the liquid-drop potential energies at the two deformations involved.

This situation can be illustrated for ^{236}U fission by reference to Figs. 4–7. For this system the liquid-drop calculation favors a total deformation of $\beta_1 + \beta_2 \simeq 1.25$ (cf. Fig. 4). The symmetric 118/118 mass split (Fig. 7) and the 132/104 mass split (Fig. 6) both have secondary minima in their potential energy surfaces close to the total deformation of 1.25 favored by the liquid drop in addition to the one favored at low E^*. In the case of the symmetric mass split (Fig. 7) the system relaxes with increasing E^* toward a smaller total deformation (i.e., from point Y to point X) while for the 132/104 and 140/96 mass splits, the relaxation is toward a larger deformation. This leads to the expectation that for $\tau_{\text{int}} \gtrsim 0.7$ MeV the TKE for symmetric mass splits in ^{236}U should increase with increasing E^* and decrease for the 132/104 and 140/96 mass splits. This effect should be especially large for mass splits near $A_H = 132$ because of the large difference in the liquid-drop potential energy between the low-E^*, shell-stabilized configuration ($\beta_1 + \beta_2 \approx 0.95$) and the configuration of the secondary minimum ($\beta_1 + \beta_2 \approx 1.4$). The difference in the liquid-drop potential energies for these two minima, seen in Fig. 6, can be estimated by referring back to Fig. 4 at the appropriate deformations. Clearly the strength of the shell correction for the configuration ($\beta_1 + \beta_2 \approx 0.95$) is very much larger, and thus a reduction in the shell corrections with increasing E^* proportional to the shell strength must lead to the relative enhancement of the configuration at the secondary minimum. For the 140/96 mass split, no secondary shell is available and the relaxation should occur more slowly. Experimental data on the excitation-energy dependence of TKE for various mass splits in the proton-induced fission of ^{233}U, ^{235}U, and ^{238}U have been obtained by Ferguson *et al.*[45] All the systems show similar behavior, and the ^{233}U(p,f) data are reproduced in Fig. 25. The dependence is just that expected from the shell-correction analysis presented above. Such data are particularly useful since they give in-

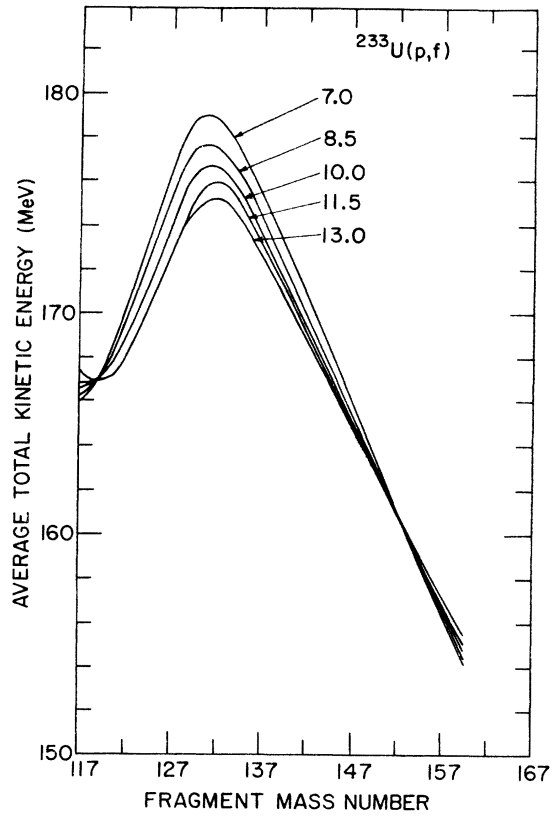

FIG. 25. The experimental values of the total kinetic energy for the system $^{233}U(p,f)$ at various proton bombarding energies [from Ferguson *et al.* (Ref. 45)]. These data are for "provisional masses" with no correction included for neutron emission.

formation on the difference in total deformation between the shell-stabilized and liquid-drop favored configurations and, hence, on scission shapes as a function of E^* and mass split. Moreover, with suitable corrections to the experimental data for multichance fission and neutron evaporation, the observed E^* dependence may yield information on the rate at which the shell corrections are diminished and, hence, on τ_{int} at the scission point.

Additional experimental evidence bearing on the above analysis has recently been obtained by Roche *et al.*[46] who measured fission-fragment mass and kinetic energy distributions for (d,p)-induced fission of ^{229}Th, ^{239}Pu, and ^{249}Cf as a function of E^* of the compound nucleus in the range 4.5–10.0 MeV. Essentially no change in TKE for several different ranges of fragment mass was observed in the case of ^{230}Th for an ~4 MeV change in E^*. For ^{240}Pu and ^{250}Cf, they observed a fairly rapid decrease in TKE for mass splits involving $A_H \sim 132$ and a slower decrease for mass splits involving $A_H \sim 142$. These data are consistent with the analysis given above, except for the mass split involving $A_H \sim 142$ in ^{250}Cf. As discussed in Sec. III B on mass distributions, τ_{int} at the scission point is expected to increase with the Z^2/A of the fissioning system. The ^{230}Th system (at low Z^2/A) is expected to have a low τ_{int} at scission. With small increases in E^*, the shell corrections which contribute importantly to the potential energy calculation are not expected to change significantly (cf. Fig. 3). The observation that TKE for ^{230}Th does not change with small increases in E^* may, indeed, be evidence for estimating the value of τ_{int} at scission (i.e., ~0.4 MeV). Both ^{240}Pu and ^{250}Cf (with expected higher values of τ_{int}) should show an E^* dependence. The mass splits involving $A_H \sim 132$ should show a rapid decrease in TKE with increasing E^* as discussed for ^{236}U above. The analysis would predict for the splits involving $A_H \sim 142$ that in ^{240}Pu the TKE should decrease more slowly with E^*, as observed. This is again analogous to the 140/96 mass split in ^{236}U discussed above. In the case of ^{250}Cf the neutron number is just at the edge of the rapid transition in deformation expected for the complement of the $A_H \sim 142$ fragment (i.e., the transition from B to C in Fig. 1 or in the region of $N_L \sim 64$ in Fig. 22). The total deformation of the 142/108 mass split in ^{250}Cf is expected to be close to that of the liquid-drop value, and no change or a slight increase in TKE with increasing E^* would be predicted. However, a decrease is observed. A more definitive test would be provided by data for mass splits involving $A_H \sim 142$ in a system with more neutrons, such as ^{252}Cf or an isotope of Fm, which would move the N_L value of the complementary mass away from the transition region.

C. Width of total kinetic energy distributions

Another interesting feature of the fission process is observed in measurements of the root-mean-square width of the total kinetic energy release as a function of fragment mass σ_A(TKE). A peak in the distribution of σ_A(TKE) has been attributed to the overlap of the "symmetric" and "asymmetric" TKE distributions in a "two-mode" analysis of fission.[47] A recent detailed study of the energetics of fission in a number of fissioning systems[33,48] reveals an interesting pattern in the structure of σ_A(TKE). These data are plotted in Fig. 26 as a function of the fragment mass along with data on ^{226}Re(p,f).[38] Three of the systems (^{227}Ac, ^{252}Cf, and ^{255}Es) show a peak in σ_A(TKE) at mass number 130. ^{230}Th, ^{236}U, ^{246}Cm, and ^{252}Cf all show a peak at $A = 123$. A third coincidence of peaks occurs in the mass

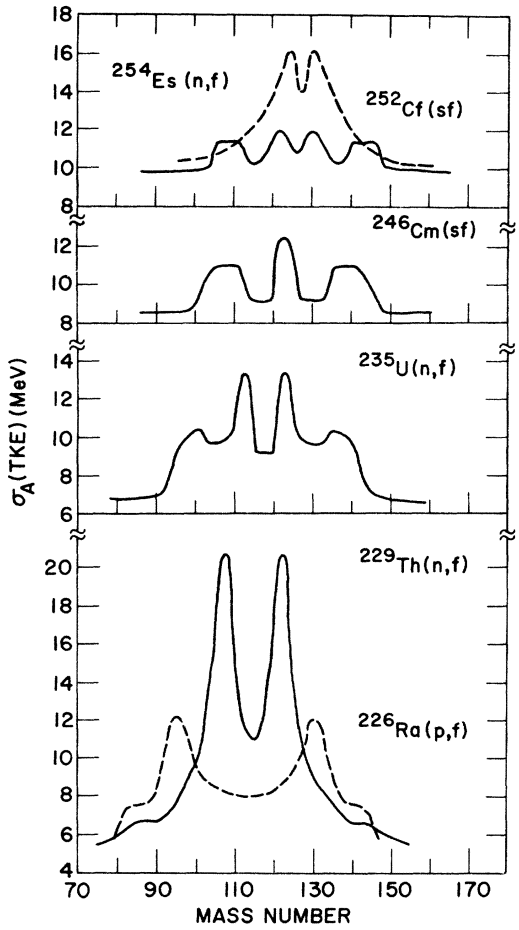

FIG. 26. The rms width of the total kinetic energy distribution as a function of the fragment mass for various fissioning systems.

region $105 \leq A \leq 111$ for ^{230}Th, ^{246}Cm, and ^{252}Cf with the ^{230}Th peak being intense, narrow, and centered in this mass range.

Calculations of σ_A(TKE) from our model are consistently smaller than observed. However, as pointed our previously, the model assumes a single value for the parameters and, realistically, some dispersion in these should be included. In particular, a dispersion in the parameter d (the distance between the ends of the spheroids) would directly affect the TKE and increase σ_A(TKE). The presence of structure in σ_A(TKE) should be independent of the absolute value of σ_A(TKE) and can be qualitatively understood as resulting from comparable contributions to the formation of a given mass split from configurations of different total deformation. The occurrence of peaks at the same mass number in different fissioning systems indicates that the effect is very likely the result of competing deformed-shell corrections at these masses and/or their complements. For simplicity, we shall again use only the neutron-shell correction whenever possible to illustrate our interpretation of the data. The complete potential energy calculation does, of course, involve all the terms of Eq. (1), with the yields calculated from Eq. (2).

For the N/Z ratios appropriate to the fissioning systems of Fig. 26, the mass numbers 130, 123, and ~108 correspond to neutron numbers (N) of ~80, ~75, and ~66, respectively. From Fig. 1 it can be seen that at $N \sim 80$, three possible deformations compete—namely, at $\beta \approx 0.1$, 0.5, and 0.85. In the case of the ^{227}Ac compound nucleus, the complement of $A_H = 130$ is $A_L = 97$ with $N_L \sim 58$. This neutron number has two competing shell-correction minima at $\beta \sim 0.4$ (point B) and $\beta \sim 0.85$ (near point E). The most probable competition is between configurations with $\beta_L \sim 0.4$, $\beta_H \sim 0.85$ (points B and K) and $\beta_L \sim 0.85$, $\beta_H \sim 0.1$ (point E and near G). The large σ_A(TKE) seen at $A_H = 130$, then, is the result of comparable yields from configurations varying in total deformation $(\beta_L + \beta_H)$ from ~0.95 to 1.25. At ^{230}Th the addition of two neutrons to the light fragment complement of $A_H = 130$, shifts the neutron-shell correction minimum away from point B and toward point E. Hence, the configurations $\beta_L \sim 0.85$ (at point E) and $\beta_H \sim 0.1$ (near point G) now dominate the yield at $A_H \sim 130$ and the corresponding σ_{130}(TKE) for ^{230}Th is small. A peak in σ_{130}(TKE) again appears in ^{252}Cf where the deformation at point K ($\beta_H \sim 0.85$) competes with that near point G ($\beta_H \sim 0.1$). The former combines with $\beta_L \sim 0.47$ at $N_L \sim 75$ and the latter with $\beta_L \sim 0.9$ to give a total deformation $(\beta_L + \beta_H)$ varying between ~1.32 and ~1.0. The structure at $A = 130$ is also present in ^{255}Es fission and is evident in the data for ^{257}Fm(sf) (Ref. 42) and ^{257}Fm(n,f) (Ref. 35) which show an increasingly large spread in TKE at this mass. The effect should be a maximum at ^{260}Fm with an exceptionally large value of σ_{130}(TKE) resulting from various combinations of the deformations of both fragments among $\beta \approx 0.1$, 0.5, and 0.85.

The structure in σ_A(TKE) at mass number ~123 for ^{252}Cf is principally a reflection of the structure discussed above at $A \approx 130$. For the systems ^{230}Th, ^{236}U, and ^{246}Cm, the peak in σ_{123}(TKE) is the result of competition between comparable shell corrections at $N \sim 75$. This is not so obvious from Fig. 1 alone; however, if both proton- and neutron-shell corrections are considered (at $Z \sim 48$, $N \sim 75$), competitive regions occur at $\beta = 0.47$ and 0.77. For ^{246}Cm, $A = 123$ represents a symmetric split for which the deformations $(\beta_1 + \beta_2) = 1.24$ and $(\beta_1 + \beta_2) = 1.54$ are the principle configurations. The value of σ_A(TKE) data is well

illustrated in this example. Such data can serve as an indicator that shell-correction minima at different deformations must be present in comparable strength in a particular mass region even though none of them is especially probable in total fission yield.

The peak in σ(TKE) centered at $A \approx 108$ in ^{230}Th, ^{246}Cm, and ^{252}Cf should be associated with neutron number $N_L \approx 66$. Figure 1 indicates only one strong shell-correction minimum for neutron numbers near this value near point C ($\beta \sim 0.6$). Our interpretation of the σ_A(TKE) data suggests another competing shell should be present, however. Some additional considerations make such a conclusion plausible. The neutron-emission function for ^{252}Cf, e.g., indicates that a fragment in the mass range $A_L \approx 108$ is not highly deformed, thus the competing shell correction we seek should be at relatively low β. In the discussion of mass distributions (Sec. III B) it was pointed out that for neutron numbers ~54–68 in Fig. 1 at $\beta \sim 0.3$ and/or proton numbers ~35–44 in Fig. 2 at the same β, an increase in the shell correction would be more consistent with the data. Such an increase is now also seen to be consistent with the σ(TKE) data and provides the alternate configuration needed.

For ^{246}Cm and ^{252}Cf the configurations contributing to σ_{108}(TKE) are $\beta_H \sim 0.65$ (point H) with $\beta_L \sim 0.6$ and ~0.3. The exceptionally large value for σ_{108}(TKE) for ^{230}Th is understood in terms of two alternatives in the deformation at $N \sim 66$ being in phase with two alternatives in the complement at $N \sim 74$ (i.e., $\beta_L \sim 0.3$ and ~0.6 with $\beta_H \sim 0.47$ and 0.77). The combination of four configurations with comparable probability of formation leads to a large spread in total deformation and, hence, to a large σ(TKE).

The qualitative arguments presented above are useful in providing a simple interpretation of experimental data in terms of the dominant role of the deformed-shell corrections of Figs. 1 and 2. However, the relative contributions of competing configurations must be determined from the full potential energy and yield calculations of Eqs. (1) and (2). Such a calculation is illustrated in Fig. 27 for ^{236}U. The distance between charge centers D is given (in fm) as a function of the fragment mass number. The contour lines connect points of equal fractions of the most probable yield for each mass split. Thus, the black areas represent the yield between the most probable yield Y_{max} and $0.75Y_{max}$, the cross-hatched area that between $0.75Y_{max}$ and $0.50Y_{max}$, and the vertical-striped area that between $0.50Y_{max}$ and $0.25Y_{max}$. The open areas represent yields below 0.25_{max} for each mass split. The effect of a variation in D on the observed width of the TKE distribution for any mass split can be judged by the relative yield values. Thus, the largest effect is expected near $A_H \approx 123$ and a somewhat smaller effect near $A_H \approx 135$. These locations are marked by arrows in Fig. 27 and agree very well with the relative heights and locations of the observed σ(TKE) data for ^{235}U(n,f) given in Fig. 26. The minima observed in the data of Fig. 26 are also consistent with the regions of small variation in D from Fig. 27.

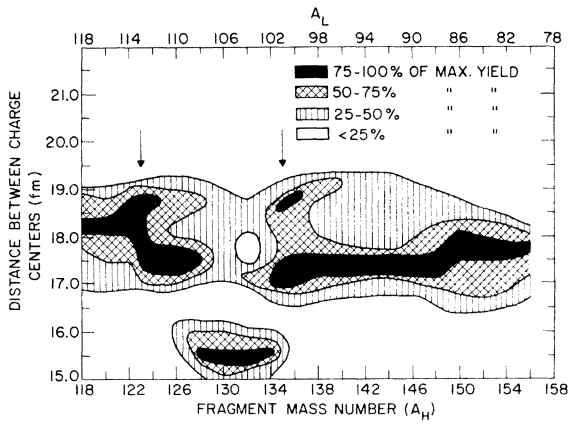

FIG. 27. A plot of the calculated yield as a function of the distance between charge centers for different mass splits in the system ^{236}U. The lines join points of equal percentage yield (25, 50, and 75%) relative to the maximum yield calculated for the distribution of D values at each mass split. No direct comparison can be made in this figure between the absolute yields of different mass splits. The arrows indicate the positions of peaks in the experimental data on σ_A (TKE) for ^{235}U (n,f) seen in Fig. 26.

An excitation energy dependence of σ_A(TKE) is also expected. This should be especially pronounced for mass splits where a second shell correction at different total deformation becomes more probable as E^* increases. For mass splits near $A = 132$, this effect is particularly prominent (as discussed in Sec. IV B above) and should lead to the development of a peak in σ_{132}(TKE) with increasing E^*. This can be seen in the data on charged-particle fission of U isotopes, for example.[45] On the other hand, if a peak in σ_A(TKE) is present at low E^*, it would decrease with increasing E^* if one of the competing configurations were to become dominant.

V. RADIUM THRESHOLD ANOMALY AND PRESCISSION KINETIC ENERGY

Konecny, Specht, and Weber[49] have observed a difference of 1–2 MeV in the fission thresholds for asymmetric and symmetric mass splits in a

study of the excitation functions for several radium and actinium isotopes. This observation suggests the possibility of different saddle points for asymmetric and symmetric fission "modes" and that the mass split is determined at the saddle point. However, an interpretation of this result, consistent with our scission-point model, is also possible.

The total available energy release at the scission point comprises mainly the Coulomb interaction energy (V_C), the deformation energies of the two fragments (E_{def}), the intrinsic excitation energies of the fragments (E_{int}), and any precission kinetic energy (E_{pre}). The total kinetic energy, approximated by (V_C+E_{pre}), is known to decrease slowly as the mass of the fissioning system decreases, while the total energy release between the saddle point and the separated fragments at infinity (Q_{saddle}) decreases much more rapidly. Within the framework of our model, E_{def} and V_C are determined at the scission point and are independent of Q_{saddle}. Thus, a decreasing Q_{saddle} should be reflected in a decrease in the sum of E_{int} and E_{pre}. For a sufficiently small fissioning mass, the saddle-point and scission-point energies approach each other and the sum $E_{int}+E_{pre}$ approaches zero.

If the minimum potential energy [Eq. (1)] associated with the scission configuration lies above the saddle-point energy for a particular mass split, then a fission threshold at some excitation energy above the saddle-point barrier will appear for that mass split. Such a threshold would be expected to occur only for those fissioning systems in which $E_{int}+E_{pre}\approx 0$. For systems of larger Z^2/A for which the minimum potential energy at the scission point for all mass splits lies well below the saddle-point energy (i.e., $E_{int}+E_{pre}>0$) no such threshold occurs and the yield for any mass split can be calculated from Eq. (2).

Our analysis of the total kinetic energy data for ^{227}Ra fission has indicated that the experimental TKE can be fitted with a value of d (the distance between the tips of the spheroids at the scission point) of 2.0 fm (cf. Sec. IV B). Experimental TKE data[49] and calculated values of V_C are compared in Fig. 28(a). The latter are calculated at each mass split for the scission shape associated with the minimum potential energy (V_{min}) of Eq. (1) using $d=2.0$ fm. The Coulomb energy, V_C, is expected to overestimate slightly the TKE owing to small amounts of the Coulomb interaction energy being converted into excitation energy of the fragments. Approximately 2 MeV should be added to the experimental data to correct for neutron emission. This would bring the observed and calculated result into excellent agreement and indicates that the distance between the charge centers at the

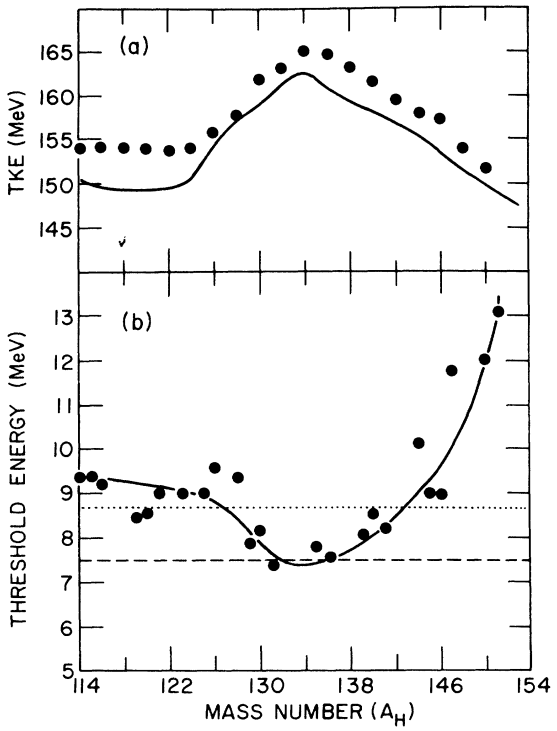

FIG. 28. (a) Comparison of the experimental TKE data for ^{227}Ac (Ref. 49) (solid line) with the calculated Coulomb energy V_C (points) for ^{227}Ra. (b) The calculated threshold energy for different mass splits in the system ^{227}Ra. The dashed line is the approximate experimental saddle-point barrier, while the dotted line represents an available energy which separates symmetric from asymmetric mass splits. The solid line is drawn only to guide the eye. The calculations shown in this figure were carried out with $\tau_{int}=0$.

scission point is being calculated correctly. The energy difference between the ground state of ^{227}Ra and the scission configuration at each mass split associated with V_{min} from Eq. (1) (i.e., the threshold energy calculated at $\tau_{int}=0$) is given in Fig. 28(b). The saddle-point barrier is known to be ~7.5 MeV for this system[49] and is indicated by a dashed, horizontal line in Fig. 28(b). A horizontal, dotted line representing the available energy in this fissioning system is arbitrarily drawn at 8.7 MeV. This line is seen to separate symmetric and asymmetric mass splits. The formation of mass splits above the dotted line is inhibited since the minimum value for the sum ($E_{def}+V_C$) for these splits is greater than the available energy. This analysis is consistent with the observations of a separate "symmetric threshold" above the fission barrier for masses between ~105 and 123,[49] and, moreover, indicates a similar threshold should exist for very asymmetric splits ($A_H\gtrsim 145$). The most probable asymmetric splits

($123 \leq A_H \leq 145$) experience the usual threshold and excitation function associated with the fission barrier. It should be noted that mass splits which include an odd-odd fragment will lie ~2 MeV above the curve shown in Fig. 28(b), and would be expected to show an even higher threshold energy.

Also, the difference in slopes of the excitation functions for symmetric and asymmetric splits observed in the studies of Konecny *et al.*[49] in the region just above the thresholds ($7 \lesssim E^* \lesssim 15$ MeV) can be understood in terms of the energy dependence of the fragment shells. This energy region corresponds to values of E_{int} between 0 and ~8 MeV or $\tau_{\text{int}} \lesssim 0.6$ MeV.

In the fission of radium isotopes, the potential energy minimum for symmetric mass splits occurs for $N \sim 70$, $\beta \sim 0.6$–0.7 (cf. Fig. 1). This is close to the location of a strong shell at $N = 65$, $\beta = 0.6$ (point C, Fig. 1). As illustrated in Fig. 3, the energy dependence of the shell correction at a given deformation is a function of the neutron number. In the excitation energy region of interest above the radium fission thresholds, configurations with several neutrons away from the strongest shell show an *increase* in shell strength with increasing excitation energy. The average shell correction for symmetric splits in radium fission (with $N \sim 70$) is expected to show this behavior for a range τ_{int} from ~0.4 to ~0.8 MeV.

The average shell corrections for the asymmetric splits in the radium region are dominated by points G and H of Fig. 1. These are strong shells, and the excitation energy dependence shown for $N = 88$ in Fig. 3 is that of point H, with the strength *decreasing* as τ_{int} increases above 0.4 MeV. The same dependence is expected for the $N = 82$ shell at $\beta \sim 0.1$ (point G). This difference in energy dependence for the shell corrections accounts for the observed relative enhancement of symmetric fission with increasing E^* in radium fission at these low values of τ_{int}. Of course, further increase in E^*, to values where the shell corrections are substantially reduced and the liquid-drop behavior begins to dominate, lead to a continued enhancement of symmetric over asymmetric fission.

We believe that the above interpretation of the "radium threshold anomaly" is plausible and consistent with our scission-point model of fission. It implies that for nuclei such as ^{226}Ra the saddle point and scission point may be essentially at the same energy, whereas in more fissionable species, the energy difference between the saddle and scission points increases with Z^2/A. This is also consistent with our previous remarks regarding viscous heating during the path from saddle to scission and the increase in τ_{int} with Z^2/A of the fissioning nucleus. This interpretation of the threshold anomaly also implies, in principle, a different threshold for each mass split for which the minimum potential energy lies above the saddle-point energy. This may be difficult to observe experimentally, however, owing to limitations in mass resolution and statistics. Moreover, since this condition will be satisfied by only a narrow region of shapes at excitation energies just above the "symmetric threshold," the width of the total kinetic energy variation for such splits should be very narrow. Data such as that observed by Konecny *et al.*[49] should, then, be very useful in establishing the shape of the nucleus at the scission point.

The observed kinetic energy of fission fragments is the sum of the Coulomb repulsion at scission and any prescission kinetic energy developed in the fissioning system between the saddle and scission points. A knowledge of the shape of the system at scission is needed to determine the division of kinetic energy between these two forms. A near spherical shape for mass number 132 is probably the best established fission fragment configuration at low excitation energies. Any structure in the experimental data on TKE as a function of the fissioning system for mass splits with $A = 132$ for one of the fragments should reflect the shape of the complementary fragment.

In our model, the Coulomb energy is calculated from Eq. (4), with D given by,

$$D = k_1(\beta_1) r_0 A_1^{1/3} \left(1 + \frac{2\beta_1}{3}\right) + k_2(\beta_2) r_0 A_2^{1/3} \left(1 + \frac{2\beta_2}{3}\right) + d \,. \tag{14}$$

For the mass splits involving nearly spherical fragment at $A = 132$ ($\beta_2 = 0.05$), Eq. (14) can be solved for the deformation of the complementary fragment (β_1) with $d = 1.4$ fm and D determined from Eq. (4) and the experimental TKE for this mass split. This calculation assumes no prescission kinetic energy. The points in Fig. 29 represent the result of such calculations for different fissioning systems, plotted as the sum of the total fragment deformation ($\beta_1 + \beta_2$). A calculated value for ($\beta_1 + \beta_2$) for each fissioning system is also derived from our model directly from considerations of the minimum potential energy for the appropriate mass split. This "theoretical" value is plotted as a solid curve in Fig. 29. The theoretical line and "experimental" data should be compared at equivalent scission-point excitation energies (E^*), but the latter are not well known. The experimental points are seen to follow the general structure trends in the calculated curve. However,

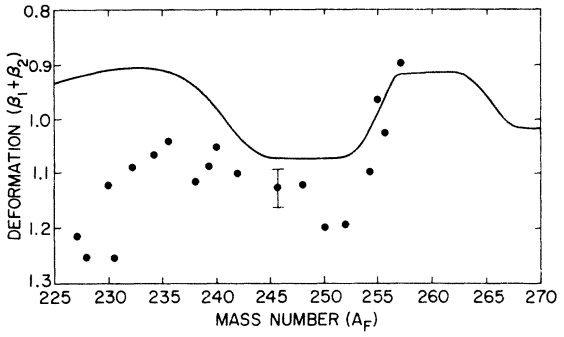

FIG. 29. A comparison of "theoretical" and "experimental" values of total deformation as a function of A_F. The solid line represents the calculated deformation coordinate $(\beta_1+\beta_2)$ of the potential energy minimum associated with the mass configuration (132+ complement) as a function of the fissioning system A_F. The points represent, for the same mass configurations, the deformation inferred from the experimental value of the TKE (see text). An error bar is given on one of the points showing a typical spread in deformation due to the quoted uncertainty in the experimental value of TKE.

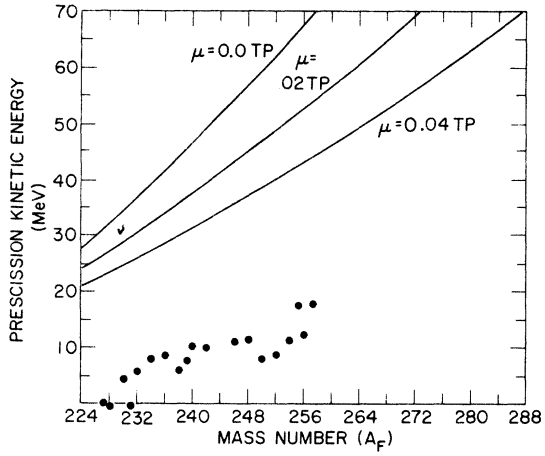

FIG. 30. Prescission kinetic energy as a function of A_F. The points represent estimates of the prescission kinetic energy based on the scission shapes derived from our model. The solid lines are the calculated prescission kinetic energies for three different values of the viscosity coefficient as obtained in the dynamic calculation of Davies *et al.* (Ref. 40).

there is a discrepancy in the values of $(\beta_1+\beta_2)$ between the two that diminishes with increasing A_F.

The discrepancy may be removed by adjustments in the value of d (the separation distance between the tips of the spheroids at scission) for each system. However, this would lead to a decreasing value of d with increasing Z^2/A of the system in conflict with the calculations of Cohen and Swiatecki.[50] They found d, in a two-spheroid model, to be a slightly increasing function of A_F in order to fit the scission-point energies for Frankel-Metropolis shapes. A constant value of $d=2.0$ fm is consistent with their results and would lead to new values of $(\beta_1+\beta_2)$ from the experimental TKE data which lie above the curve in Fig. 29, i.e., at lower $(\beta_1+\beta_2)$. This value of d is also consistent with the analysis of the radium threshold anomaly given above. If it is assumed that the calculation with $d=2.0$ fm yields the correct scission shapes in our model, then the difference between the total deformation derived from the experimental TKE data and that calculated from the model can be converted to an equivalent difference in kinetic energy. This difference in energy can be ascribed to prescission kinetic energy and is plotted in Fig. 30 along with estimates from the dynamic calculations of Davies *et al.*[40] Our estimated prescission kinetic energies increase with A_F from a value near zero in the radium region.

The much smaller values for the prescission kinetic energy derived from the scission shapes given by our model are consistent with the narrow angular distributions observed in long-range α-accompanied fission[51,52] and with expectations of relatively high nuclear viscosity as suggested by Swiatecki.[53] Recent calculations of nuclear viscosity based on one-body dissipative forces between the nucleons and the moving potential wall[54,55] indicate values of the prescission kinetic energy and compact scission shapes which are consistent with the results derived from the static, two-spheroid model discussed here.

VI. NUCLEAR CHARGE DISTRIBUTION

Several calculations of nuclear charge distribution in fission have been published.[56-58] In our model, the distribution in nuclear charge for any given mass split is obtained directly from Eqs. (1) and (2). As in the case of the mass distributions, the calculated charge distribution is dependent on the configurations at the scission point.

Experimental data on charge distribution have been obtained from determinations of independent yields of fission products by radiochemical methods,[59,60] K x-ray measurements,[37] the intensity of 2+ to 0+ ground-state-based transitions,[61] the number of β rays emitted from mass-separated products,[62,63] and the energy loss of mass- and energy-separated products.[64,65] Such measurements establish the most probable charge for a given mass, $Z_p(A)$ [or the average charge, $\bar{Z}(A)$, if the distribution is not Gaussian] and the width of the distribution $\sigma_Z(A)$. These are difficult mea-

surements, and each method has its own limitations in range of applicability, accuracy and resolution.

The dependence of the most probable charge on mass split is generally plotted as the quantity $(Z_p - Z_{UCD})$, where Z_{UCD} refers to the unchanged charge distribution (i.e., the same Z/A as the fissioning nucleus).

Figure 31 shows a curve (labeled Q) which gives $(\overline{Z} - Z_{UCD})$ as a function of mass split, where $\overline{Z}$ (or Z_p) is defined as the charge division leading to the maximum energy release in the formation of odd-mass fragments in their ground states in the thermal neutron fission of ^{235}U.[37] A shaded area which outlines the assessed limits to the experimental data obtained from K x-ray emission,[37] and solid circles representing calculations from our model are also given in the figure. The curve for maximum energy release (Q) represents the system with the fragments in their ground states and at infinite separation and is, of course, expected to differ from our scission-point calculation.

The calculation of charge distribution is particularly sensitive to the distance between charge centers at the scission point. The values in Fig. 31 are calculated with $d = 1.4$ fm. As stated earlier, it is our intent to utilize the same set of parameters d, τ_{int}, and T_{coll} for all calculations to assess the general applicability of the model. There are some indications from kinetic energy data in the fission of nuclei in the radium region that a value of $d = 2.0$ fm would give a better fit to the data. This is apparently the case for the charge distribution data of Fig. 31 as well, since such a change would move the calculated points toward the Q curve ~0.1 unit in $(\overline{Z} - Z_{UCD})$ and bring them into better agreement with the shaded area.

An outstanding feature of the calculated charge distribution data is the prominent fine structure. In a recent set of experiments, Clerc *et al.*[65] have obtained data on the charge distribution of mass-separated light fission products in ^{235}U thermal-neutron fission at the most probable kinetic energy. These data have sufficient resolution to observe any fine structure in the $(\overline{Z} - Z_{UCD})$ distribution. Their results are plotted in Fig. 32 along with the calculations from our model. Both sets of points are joined by lines simply to guide the eye. The correlation in the structure between experiment and calculation is striking. Clerc *et al.*[65] point out the difficulty of making a correction for neutron emission to obtain $(\overline{Z} - Z_{UCD})$ for the primary fission fragments. This leads to a possible error of as much as 0.28 units in the value of $(\overline{Z} - Z_{UCD})$ for mass splits away from the most probable. The error is such that the very asymmetric splits would be lowered on the plot [i.e., moved toward $(\overline{Z} - Z_{UCD}) = 0$] and the more symmetric splits raised on the plot (i.e., toward larger negative values). As pointed out above, the use of $d = 2.0$ fm in the calculation rather than 1.4 fm would raise the calculated points on the plot, bringing them into closer agreement with the data. Neither of the corrections would affect the character of the fine structure, however.

The peaks in $(\overline{Z} - Z_{UCD})$ which occur every 5 mass units are a result of proton pairing. At

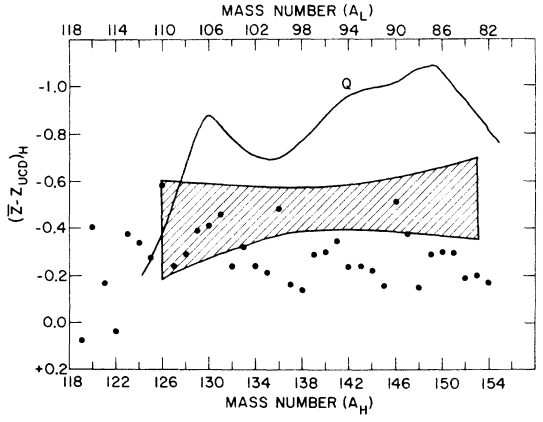

FIG. 31. A plot of $(\overline{Z}-Z_{UCD})$ as a function of mass split for the system ^{236}U. The points are calculated from our model. The elongated box encloses the data of Reisdorf *et al.* (Ref. 37), obtained from K x rays. The solid line (Q) gives the nuclear chage division associated with the maximum energy release for odd-mass fragments (see text).

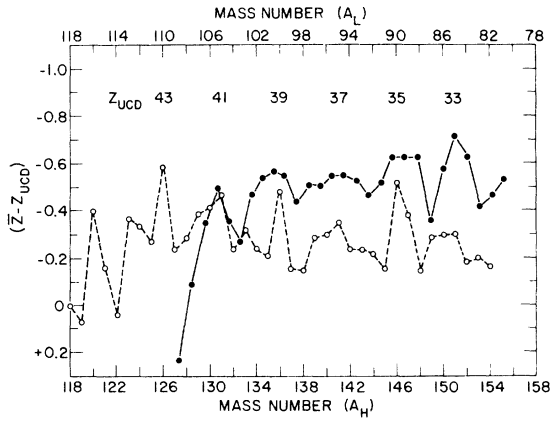

FIG. 32. The quantity $(\overline{Z}-Z_{UCD})$ for different mass splits in the fissioning system ^{236}U as calculated from our model (dashed line) compared with the experimental results of Clerc *et al.* (Ref. 65) for $^{235}U(n_{th},f)$ (solid line). The locations of the odd values of Z_{UCD} are shown in the figure.

these points the value of Z_{UCD} is very near an odd Z. Since the pairing correction favors the production of even-Z fragments, the largest difference between $\overline{Z}$ and Z_{UCD} will occur when Z_{UCD} is odd. The calculated fine structure in $(\overline{Z} - Z_{UCD})$ is seen to alternate between narrow and wide peaks. The narrow peaks occur for odd-odd fragments and the wider, less pronounced ones occur where Z_{UCD} is odd, but the neutron number is even. Structural effects are also seen in the dispersion around $\overline{Z}$ in the experimental data of Clerc *et al.*[65] as well as in the calculations of our model. When $\overline{Z}$ is close to an even value of Z, the dispersion is very narrow, whereas it is much broader when $\overline{Z}$ is near an odd value of Z, again reflecting the effect of the pairing correction.

It was pointed out earlier in this paper that the neutron-shell correction is generally stronger than the proton-shell correction and is thus the dominant factor in determining the most probable deformation of the fragment at the scission point. It was also noted that the pairing corrections are out of phase with the shell corrections, i.e., large shell corrections are associated with small pairing corrections and vice versa. These observations readily explain the strong odd-even proton effect and much weaker odd-even neutron effect seen in the experimental data.[65,66] The odd-even effects in Z and N can be correlated with the calculated total proton- and neutron-shell corrections for complementary, primary fragments. The data of Clerc *et al.*[65] for $^{235}U(n,f)$ are shown in Figs. 33 and 34. We have made a small adjustment in the neutron scale (upper abscissa in Fig. 33) using

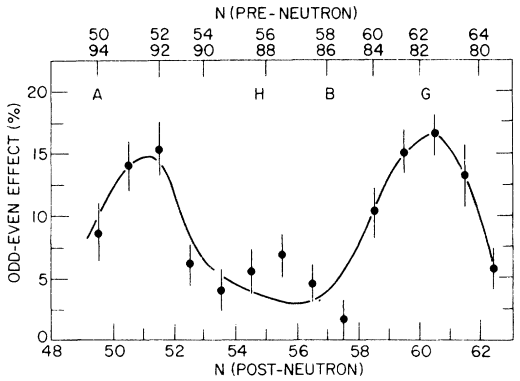

FIG. 33. The odd-even effect for neutrons as calculated by Clerc *et al.* (Ref. 65) from their experimental data on the fissioning system $^{235}U(n_{th},f)$. The upper abscissa gives the neutron number of the primary fragments estimated from the neutron emission curve. The letters refer to the location of the major neutron shells which, according to our model, play an important role in the fission of ^{236}U: these correspond to the designations of the shell corrections in Fig. 1.

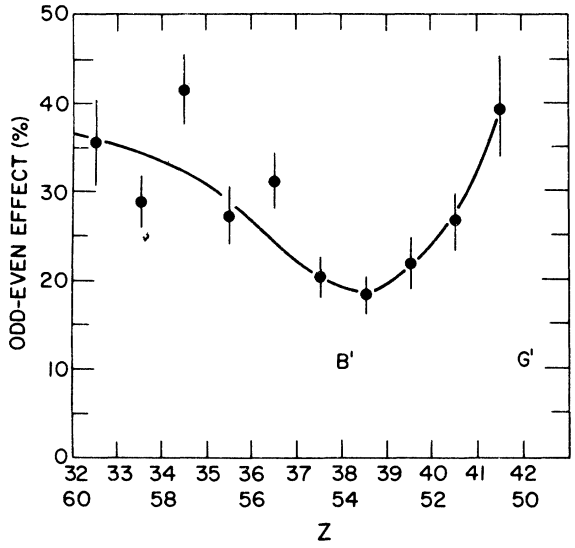

FIG. 34. The odd-even effect for protons as calculated by Clerc *et al.* (Ref. 65) from their experimental data on the fissioning system $^{235}U(n_{th},f)$. The letters refer to the location of the two major proton shells (cf. Fig. 2) which according to our model, play an important role in the fission of ^{236}U.

the experimental neutron-emission curve so that the data can be compared more directly with the neutron numbers of the primary fragments given by the calculations of our model. The letters in Figs. 33 and 34 identify the location of the strong shell corrections (and, hence, weak pairing corrections) and correspond to the lettered regions in Figs. 1 and 2. Except for the locations G and G′ in Figs. 33 and 34, regions of small odd-even effect correlate very well with the strong shell correction (or weak pairing correction) regions of Figs. 1 and 2.

This interpretation of the odd-even effects leads to some interesting predictions for other fissioning systems. If strong shell corrections occur simultaneously in both complementary fragments, the pairing corrections will be exceptionally small for these mass splits and the odd-even effect would be expected to be much reduced. This situation should prevail for neutrons in the systems $^{238}U(n,f)$ and $^{252}Cf(sf)$ where the strong neutron shells for the most probable complementary fragments are at points H and B and at H and C in Fig. 1, respectively. Likewise, systems for which the odd-even effect for neutrons should be greater than that for protons can be identified. Such a system would require the proton-shell correction to be greater than the neutron-shell correction. Inspection of Fig. 2 suggests only one region where this may be likely for readily available

fissioning systems—namely, the region near ^{227}Ra. The proton-shell correction at point C′ ($Z = 44, \beta = 0.55$) is stronger than any neutron-shell correction with $N \approx 70$ at the same deformation. We would thus expect that the system ^{226}Ra(n,f), e.g., would exhibit a stronger odd-even effect for neutrons than for protons for mass splits near symmetry.

The discrepancy noted above in the correlation of the odd-even effect at points G and G′ of Figs. 33 and 34 with the strong shell corrections of the heavy fragment at $N = 82$ and $Z = 50$ is still in need of explanation. A small odd-even effect is expected, but a large effect is observed. The light fragment complement of the $N = 82$ fragment in the ^{236}U system is at $N = 62$ with $\beta \approx 0.9$ (cf. Fig. 1). This occurs in a region between points E and F where the shell correction is not particularly strong. The odd-even neutron effect in Fig. 33 is seen to fall off as the neutron number of the light fragment either increases or decreases toward the region of stronger shell correction at points E and F in Fig. 1. This suggests that the experimental data reflects the pairing correction of the highly deformed complement of the nearly spherical $N = 82$ fragment. It has been suggested[22] that the pairing strength may be proportional to the surface area of the fragment. This would be consistent with the highly deformed shape of the light fragment at this mass split deduced from our model and might account for the observations. It would be instructive to study the odd-even effect in systems for which the complement of the $N = 82$ fragment lies closer to points E and F in Fig. 1, e.g., in ^{229}Th(n,f) and ^{246}Cm(sf), respectively. If a reduced odd-even effect is observed in these systems for the highly deformed complements of the $N = 82$ fragment, this would be confirming evidence that the pairing correction in the highly deformed fragment in the case of ^{236}U was indeed the dominant factor in the odd-even effect observed. A similar argument would apply to the deformed complement of the $Z = 50$ fragment at point G′ in the case of proton pairing (cf. Fig. 2).

If the strength of the pairing correlation decreases rapidly at temperatures approaching the critical temperature, as calculated by Moretto,[29] the structure in Z_p seen by Clerc *et al.*[65] would be expected to be a strong function of the excitation energy at the scission point. Nifenecker *et al.*[67] have suggested that the excitation energy is at a maximum value for the most probable TKE(A) for a given mass split and falls to zero at the upper and lower limits for TKE(A). As pointed out by Clerc *et al.*[64] charge dispersion data should be useful in testing this suggestion. In addition, experiments such as those of Clerc *et al.*[65] which observe structure in $Z_p(A)$ as a function of kinetic energy would not only test the Nifenecker, *et al.* suggestion, but also provide information on the distance between fragment charge centers at scission. From the calculations of our model, it is expected that the structure in $Z_p(A)$ will diminish with increasing excitation energy and the average Z_p will move toward Z_{UCD} with increasing TKE(A) (i.e., with decreasing distance between charge centers). Experimental verification of a change in the average $Z_p(A)$ with TKE(A) would support a basic premise of our model that the distribution of nucleons between the fragments and the distance between charge centers are determined at the same time—namely, near the scission point.

The rapid increase in the strength of the pairing correlation as temperature is reduced below the critical temperature may explain the observation[33] of unusually strong odd-even effects in the TKE and mass distributions for ^{229}Th(n,f) in contrast with the more typical effects for ^{233}U(n,f). If the energy available for internal excitations at the scission point decreases as Z^2/A decreases (as discussed earlier) then at some value of Z^2/A the average temperature at the scission point must pass through the region $0.3 \lesssim T \lesssim 0.5$ MeV where the pairing correlation increases rapidly as seen in Fig. 35 taken from Moretto.[29] The observed data for ^{229}Th(n,f) and ^{233}U(n,f) suggest that the average temperature at the scission point for ^{230}Th is $\lesssim 0.4$ MeV whereas for ^{234}U the value is greater than ~0.5 MeV.

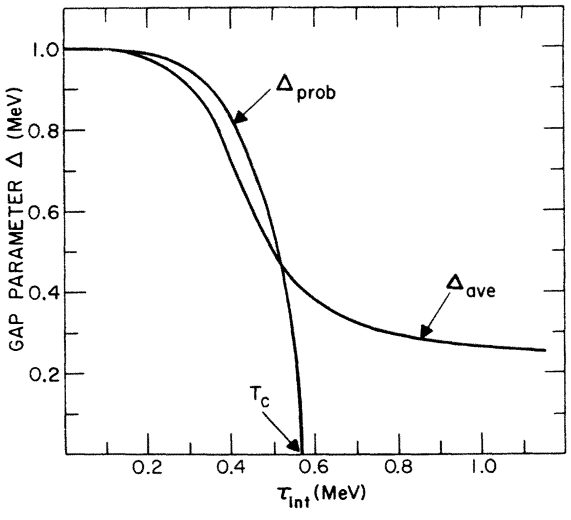

FIG. 35. The average gap parameter (Δ_{ave}) and the most probable gap parameter (Δ_{prob}) as a function of temperature [from Moretto (Ref. 29)]. The critical temperature (T_c) is at 0.57 MeV.

VII. SUMMARY AND CONCLUSIONS

We have proposed a simple, static model of nuclear fission based on the assumption of statistical equilibrium among collective degrees of freedom at the scission point. The relative probabilities of formation of complementary fission fragment pairs are determined from the relative potential energies of a system of two nearly touching, coaxial spheroids with quadrupole deformations. The total potential energy of the system at the scission point is calculated as the sum of liquid-drop and shell- and pairing-correction terms for each spheroid, and Coulomb and nuclear potential terms describing the interaction between them. Three parameters characterize the system at the scission point—the distance between the tips of the spheroids (d), the intrinsic excitation of the nascent fragments (τ_{int}), and a collective temperature (T_{coll}). No attempt has been made to adjust these parameters to give optimum fits to the experimental data. Instead, calculations for all fissioning systems have been carried out with a constant set of values for d, τ_{int}, and T_{coll}.

The general trends of the distributions of mass, nuclear charge, and kinetic energy in the fission of a wide range of nuclides from Po to Fm are well reproduced in the calculations. The major influence of the deformed-shell corrections for neutrons is pointed out and provides a convenient framework for the interpretation of observed trends in the data and for the prediction of new results.

The scission-point configurations derived from the model provide an interpretation of the saw-tooth neutron-emission curve as well as some previously unexplained observations on the variation in $\overline{\text{TKE}}$ for isotopes of U, Pu, Cm, and Cf; structure in the width of the total kinetic energy release as a function of fragment mass ratio; and a difference in threshold energies for symmetric and asymmetric mass splits in the fission of radium and actinium isotopes. The value of data on kinetic energy for particular mass splits as a function of excitation energy and fissioning species in observing specific shell effects is pointed out. Although the model does not include any dynamic considerations, the results of the calculations can be utilized, in conjunction with TKE measurements, to estimate values of the prescission kinetic energy and its dependence on the mass number of the fissioning system.

In spite of a number of recognized simplifications in the model, quantitative fits to the data are generally within expected errors of the shell corrections determined by the Strutinski prescription. Plausible explanations for discrepancies with experimental data are given. The fact that so many of the observed phenomena of fission are well reproduced in this static, scission-point model implies that the dynamics of the process in the path from saddle point to scission point either does not play a major role in the determination of the distributions calculated here or would lead to the same result.

Quantitative comparisons of the calculations with experimental data indicate that a value of $d = 2.0$ fm may be a better choice than the value of 1.4 fm used. Moreover, a variation of τ_{int} with the Z^2/A of the fissioning system should also be considered. However, until more accurate deformed-shell corrections can be determined and the effects of higher-order deformations and a normal dispersion about the parameter values are investigated, it seems premature to make such changes. The general applicability of the model to the interpretation of a wide range of fission phenomena and its utility in providing some new insight into the fission process has been successfully demonstrated. Its validity will be determined by experimental tests of its conclusions and predictions.

VIII. ACKNOWLEDGMENTS

We wish to express our appreciation to a number of colleagues at Argonne National Laboratory and elsewhere for helpful discussions and critiques of our previous interpretation of the mass and charge distributions of fission fragments.[13] In particular, the comments of W. J. Swiatecki and H. J. Krappe led to a reexamination of the basis of that calculation and to some of the changes introduced in the present extension of that model.

---

*Work performed under the auspices of the U.S. Energy Research and Development Administration.

[1]V. M. Strutinski, Nucl. Phys. A95, 420 (1967).

[2]P. Möller and S. G. Nilsson, Phys. Lett. 31B, 283 (1970).

[3]H. C. Pauli, T. Ledergerber, and M. Brack, Phys. Lett. 34B, 264 (1971).

[4]U. Mosel and H. W. Schmitt, Phys. Rev. C 4, 2185 (1971).

[5]M. G. Mustafa, U. Mosel, and H. W. Schmitt, Phys. Rev. C 7, 1519 (1973).

[6]J. Maruhn, W. Greiner, P. Lichtner, and D. Drechsel, in *Proceedings of the Third International Atomic Energy Agency Symposium on the Physics and Chemistry of*

Fission, Rochester, 1973 (International Atomic Energy Agency, Vienna, 1974), Vol. I, p. 569.
[7]P. Fong, *Statistical Theory of Nuclear Fission* (Gordon and Breach, New York, 1969).
[8]W. Nörenberg, in *Proceedings of the Second International Atomic Energy Agency Symposium on the Physics and Chemistry of Fission* (International Atomic Energy Agency, Vienna, 1969), p. 51.
[9]F. Dickmann and K. Dietrich, Nucl. Phys. A129, 241 (1969).
[10]V. V. Pashkevich, Nucl. Phys. A169, 275 (1971).
[11]H. C. Pauli and T. Ledergerber, in *Proceedings of the Third International Atomic Energy Agency Symposium on the Physics and Chemistry of Fission, Rochester, 1973* (see Ref. 6), Vol. I, p. 463.
[12]J. Maruhn and W. Greiner, Phys. Rev. Lett. 32, 548 (1974).
[13]B. D. Wilkins and E. P. Steinberg, Phys. Lett. 42B, 141 (1972).
[14]P. A. Seeger and R. C. Perisho, Los Alamos Scientific Laboratory Report No. LA-3751, September 1967 (unpublished).
[15]W. D. Myers and W. J. Swiatecki, Ann. Phys. (N.Y.) 55, 395 (1970).
[16]S. Ludwig, H. von Groote, E. Hilf, A. G. W. Cameron, and J. Truran, Nucl. Phys. A203, 627 (1973).
[17]R. W. Hasse, Ann. Phys. (N.Y.) 68, 377 (1971).
[18]S. Cohen and W. J. Swiatecki, Ann. Phys. (N.Y.) 19, 67 (1962).
[19]H. J. Krappe and J. R. Nix, in *Proceedings of the Third International Atomic Energy Agency Symposium on the Physics and Chemistry of Fission, Rochester, 1973* (see Ref. 6), Vol. I, p. 159.
[20]W. D. Myers, and W. J. Swiatecki, Nucl. Phys. 81, 1 (1966).
[21]A. C. Wahl, A. E. Norris, R. A. Rouse, and J. C. Williams, in *Proceedings of the Second International Atomic Energy Agency Symposium on the Physics and Chemistry of Fission, Vienna, 1969* (see Ref. 8), p. 813.
[22]M. Bolsterli, E. Fiset, J. R. Nix, and J. L. Norton, Phys. Rev. C 5, 1050 (1972).
[23]T. H. Braid, R. R. Chasman, J. R. Erskine, and A. M. Friedman, Phys. Rev. C 4, 247 (1971).
[24]M. Brack, J. Damgaard, H. C. Pauli, A. S. Jensen, V. M. Strutinski, and C. Y. Wong, Rev. Mod. Phys. 44, 320 (1972).
[25]P. A. Seeger, in *Proceedings of the International Conference on the Properties of Nuclei Far From Region of Beta Stability, Leysin, 1970* [CERN Report No. 70-30, Geneva, 1970 (unpublished)], p. 217.
[26]A. S. Jensen and J. Damgaard, Nucl. Phys. A203, 578 (1973).
[27]$N = N_{cl} + g_0\hbar\omega_{sh}\chi$, where N_{cl} is the number of nucleons in a closed shell, and χ is the fraction of states occupied in the next shell. $\theta = 2\pi^2\tau_{int}/\hbar\omega_{sh}$; $\chi = y - (f/2\pi g_0)\sin(2\pi y)(\theta/\sinh\theta)$.
[28]J. Bardeen, L. N. Cooper, and J. R. Schreiffer, Phys. Rev. 108, 1175 (1957).
[29]L. G. Moretto, Phys. Lett. 40B, 1 (1972).
[30]J. C. D. Milton and J. S. Fraser, Phys. Rev. 93, 818 (1954).
[31]E. K. Hyde, *The Nuclear Properties of the Heavy Elements* (Prentice-Hall, Englewood Cliffs, 1964), Vol. III.
[32]J. Terrell, Phys. Rev. 127, 880 (1962).
[33]J. P. Unik, J. E. Gindler, L. E. Glendenin, K. F. Flynn, A. Gorski, and R. K. Sjoblom, in *Proceedings of the Third International Atomic Energy Agency Symposium on the Physics and Chemistry of Fission, Rochester, 1973* (see Ref. 6), Vol. II, p. 191.
[34]H. W. Schmitt and U. Mosel, Nucl. Phys. A186, 1 (1972).
[35]W. John, E. K. Hulet, R. W. Lougheed, and J. J. Wesolowski, Phys. Rev. Lett. 27, 45 (1971).
[36]V. E. Viola, Jr., and T. Sikkeland, Phys. Rev. 130, 2044 (1963).
[37]W. Reisdorf, J. P. Unik, H. C. Griffin, and L. E. Glendenin, Nucl. Phys. A177, 337 (1971).
[38]E. Konecny and H. W. Schmitt, Phys. Rev. 172, 1213 (1968).
[39]J. Trepulka, Diploma thesis, Phys. Inst. Julius-Maximilians Univ., Würzburg, Germany, September 1969 (unpublished).
[40]K. T. R. Davies, S. E. Koonin, J. R. Nix, and A. J. Sierk, Los Alamos Scientific Laboratory Report No. LA-UR-75-5, January 1975 (unpublished).
[41]J. C. D. Milton and J. S. Fraser, Can. J. Phys. 40, 1626 (1962).
[42]J. P. Balagna, G. P. Ford, D. C. Hoffman, and J. D. Knight, Phys. Rev. Lett. 26, 145 (1971).
[43]H. W. Schmitt, J. H. Neiler, and F. J. Walter, Phys. Rev. 141, 1146 (1966).
[44]V. G. Vorob'eva, N. P. D'yachenko, N. P. Kolosov, B. D. Kuz'minov, and A. I. Sergachev, Yad. Fiz. 19, 954 (1974) [Sov. J. Nucl. Phys. 19, 489 (1974)].
[45]R. L. Ferguson, F. Plasil, F. Pleasonton, S. C. Burnett, and H. W. Schmitt, Phys. Rev. C 7, 2510 (1973).
[46]C. J. Roche, K. L. Wolf, A. J. Gorski, and J. P. Unik, Bull. Am. Phys. Soc. 21, 31 (1976); and private communication.
[47]H. C. Britt, H. E. Wegner, and J. C. Gorsky, Phys. Rev. 129, 2239 (1963).
[48]J. P. Unik (private communication).
[49]E. Konecny, H. J. Specht, and J. Weber, in *Proceedings of the Third International Atomic Energy Symposium on the Physics and Chemistry of Fission, Rochester, 1973* (see Ref. 6), Vol. II, p. 3.
[50]S. Cohen and W. J. Swiatecki, Ann. Phys. (N.Y.) 22, 406 (1963).
[51]M. J. Fluss, S. B. Kaufman, E. P. Steinberg, and B. D. Wilkins, Phys. Rev. C 7, 353 (1973).
[52]K. Tsuji, A. Katase, Y. Yoshida, T. Katayama, F. Toyofuku, and H. Yamamoto, in *Proceedings of the Third International Atomic Energy Agency Symposium on the Physics and Chemistry of Fission, Rochester, 1973* (see Ref. 6), Vol. II, p. 405.
[53]W. J. Swiatecki, J. Phys. Suppl. 33, C5-45 (1972).
[54]W. J. Swiatecki, Lawrence Berkeley Laboratory Report No. LBL-4296, 1975 (unpublished).
[55]J. Blocki *et al.*, Lawrence Berkeley Laboratory, unpublished results.
[56]W. Nörenberg, Z. Phys. 197, 246 (1966).
[57]J. Wing and P. Fong, Phys. Rev. 157, 1038 (1967).
[58]K. Gupta, W. Scheid, and W. Greiner, Phys. Rev. Lett. 35, 353 (1975).
[59]A. C. Wahl, A. E. Norris, R. A. Rouse, and J. C. Williams, in *Proceedings of the Second International Symposium on the Physics and Chemistry of Fission, Vienna, 1969* (see Ref. 8), p. 813.

[60]J.-V. Kratz and G. Hermann, in *Proceedings of the Third International Atomic Energy Agency Symposium on the Physics and Chemistry of Fission, Rochester, 1973* (see Ref. 6), Vol. II, p. 95.
[61]E. Cheifitz, J. B. Wilhelmy, R. C. Jared, and S. G. Thompson, Phys. Rev. C 4, 1913 (1971).
[62]K. Sistemich, P. Armbruster, J. Erdens, and E. Roeckl, Nucl. Phys. A139, 289 (1969).
[63]H. Gunther, G. Siegert, R. L. Ferguson, and H. Ewald, Nucl. Phys. A196, 401 (1972).
[64]H.-G. Clerc, K.-H. Schmidt, H. Wohlforth, W. Lang, H. Schrader, K. E. Pferdekämper, R. Jungmann, M. Asghar, J. P. Bocquet, and G. Siegert, Nucl. Phys. A247, 74 (1975).
[65]H.-G. Clerc, W. Lang, H. Wohlforth, K.-H. Schmidt, H. Shrader, K. E. Pferdekämper, and R. Jungmann, Z. Phys. A274, 203 (1975).
[66]S. Amiel and H. Feldstein, Phys. Rev. C 11, 845 (1975).
[67]H. Nifenecker, C. Signarbieux, R. Babinet, and J. Poitou, in *Proceedings of the Third International Atomic Energy Agency Symposium on the Physics and Chemisty of Fission, Rochester, 1973* (see Ref. 6), Vol. II, p. 117.